Near-surface soil moisture assimilation for quantifying effective soil hydraulic properties using genetic algorithm: 1. Conceptual modeling

Amor V. M. Ines[1,2] and Binayak P. Mohanty[1]

Received 23 February 2007; revised 11 March 2008; accepted 31 March 2008; published 27 June 2008.

[1] We used a genetic algorithm (GA) to identify soil water retention θ(h) and hydraulic conductivity K(h) functions by inverting a soil-water-atmosphere-plant (SWAP) model using observed near-surface soil moisture (0-5 cm) as search criterion. Uncertainties of parameter estimates were estimated using multipopulations in GA and considering data and modeling errors. Three hydrologic cases were considered: (1) homogenous free-draining soil column, (2) homogenous soil column with shallow water table, and (3) heterogeneous soil column under free-drainage condition, considering three different rainfall patterns in northern Texas. Results (cases 1 and 2) showed the identifiability of soil hydraulic parameters improving at coarse and fine scales of the soil textural class. Medium-textured soils posed identifiability problems when the soil is dry. Nonlinearity in θ(h) and K(h) is greater at drier conditions, and some parameters are less sensitive for estimation. Flow regimes controlled by upward fluxes were found less successful, as the information content of observed near-surface data may no longer influence the hydrologic processes in the subsurface. The identifiability of soil hydraulic parameters was found better when the soil profile is predominantly draining. In case 3, top soil layer hydraulic properties were defined using near-surface data alone as criterion. Adding evapotranspiration (ET) improved identification of the second soil layer, although not all parameters were identifiable. Under uncertainties, θ(h) was found to be well defined while K(h) is more uncertain. Finally, we applied the method to a validation site in Little Washita watershed, Oklahoma, where derived effective soil hydraulic properties closely matched the measured ones at the field site.

Citation: Ines, A. V. M., and B. P. Mohanty (2008), Near-surface soil moisture assimilation for quantifying effective soil hydraulic properties using genetic algorithm: 1. Conceptual modeling, *Water Resour. Res.*, *44*, W06422, doi:10.1029/2007WR005990.

1. Introduction

[2] As remotely sensed soil moisture data become widely available [*Kerr et al.*, 2001; *Njoku et al.*, 2003; *Entekhabi et al.*, 2004], the prospects of identifying pixel-based effective soil hydraulic parameters across the globe become more imminent in the future. Pixel-based soil hydraulic parameters are essential inputs to large-scale hydrologic and hydroclimatic models, e.g., soil-vegetation-atmosphere-transpiration (SVAT) models. Most of their subsurface flow modules are based on the Darcian flow equation that requires closed-form equations of the soil hydraulic functions (i.e., the soil water retention θ(h) and hydraulic conductivity K(h) functions, where h is the pressure head) for modeling the responses of the soil to store, release, and transmit water under different hydrologic conditions [*Demarty et al.*, 2005]. These soil hydraulic functions, on the other hand, require parameters that are distinct among soil types. At larger spatial scales, they are considered as effective parameters, as they are used to describe the heterogeneity of the landscape contained inside the pixel [*Kabat et al.*, 1997; *Feddes et al.*, 1993a, 1993b; *Zhu and Mohanty*, 2003; *Mohanty and Zhu*, 2007]. Developing robust approaches or algorithms to quantify such effective soil hydraulic parameters is of paramount importance for large-scale hydrologic and hydroclimatic model applications.

[3] Soil moisture derived from remote sensing platforms accounts only for the near-surface soil layers. The passive microwave L-band (1.4 GHz) sensor, for example, has a maximum penetration depth of 5 cm from the soil surface under minimal vegetation cover [*Jackson et al.*, 1995]. Since the root zone ($\sim$0–100 cm for grass and croplands) soil moisture is an important variable in partitioning the surface energy budget, a lot of effort have been made in using near-surface soil moisture information to retrieve soil moisture profiles in the unsaturated zone [e.g., *Entekhabi et al.*, 1994; *Galantowicz et al.*, 1999; *Walker et al.*, 2001; *Crow and Wood*, 2003; *Walker and Houser*, 2004; *Dunne and Entekhabi*, 2005]. Apparently, these studies are dedicated only to the retrieval of profile soil moisture and not for determining profile soil hydraulic properties because they are assumed to be known beforehand. *Vrugt et al.* [2005] argued that hydrologic system parameters are often not available in real-world conditions and that model

[1]Department of Biological and Agricultural Engineering, Texas A&M University, College Station, Texas, USA.

[2]Now at International Research Institute for Climate and Society, The Earth Institute at Columbia University, Palisades, New York, USA.

0043-1397/08/2007WR005990$09.00

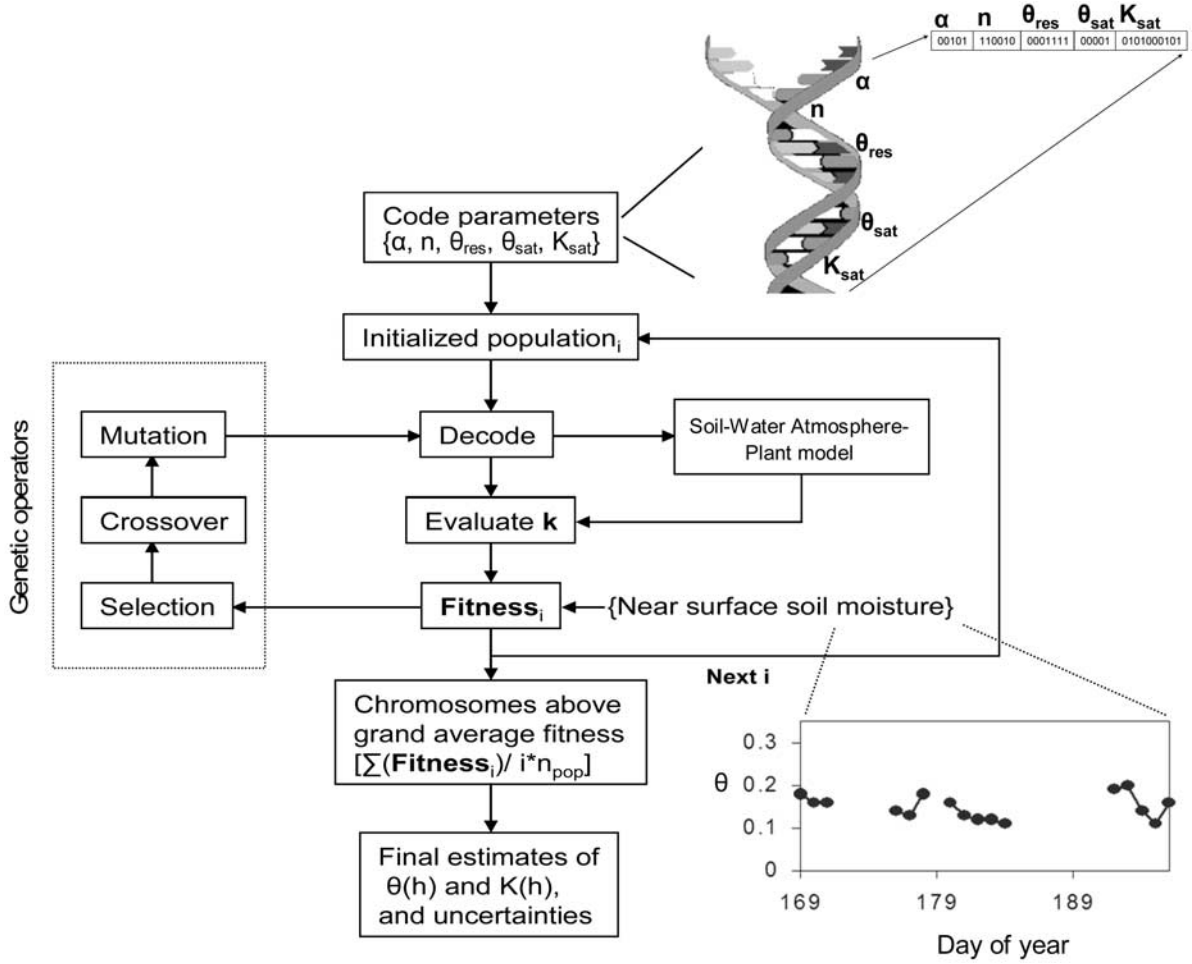

Figure 1. Schematic diagram of the genetic algorithm-based near-surface soil moisture assimilation by inverse modeling [see *Ines and Mohanty*, 2008]. Note that $\mathbf{k} = \{\mathbf{p}_{j=1,\,m-1}, \lambda\}$ if λ of the Mualem-Van Genuchten functions is fixed; $\mathbf{p}_{j=1,\,m-1} = \{\alpha, n, \theta_{res}, \theta_{sat}, K_{sat}\}$ (see section 2.1.2).

parameters should be estimated based on observed hydrological data to account for uncertainties involved in model conceptualization, e.g., those caused by spatial and process aggregation.

[4] Several studies on quantifying soil hydraulic parameters using near-surface soil moisture information have been reported in the literature, but their scope was limited for defining the hydraulic properties and processes beyond the near-surface soil layers. *Mattikalli et al.* [1998] devised regression equations to quantify effective saturated hydraulic conductivities (K_{sat}) of the Little Washita watershed in Oklahoma using temporal changes of brightness temperature and near-surface soil moisture derived from the ESTAR passive microwave sensor during the Washita'92 campaign [*Jackson et al.*, 1995]. *Burke et al.* [1997, 1998] coupled a microwave emission model with a soil-water-energy and transpiration model to quantify soil hydraulic properties by calibrating the Campbell soil hydraulic parameters [*Campbell*, 1974] until the cumulative error between the observed and simulated brightness temperatures is minimized. The derived soil hydraulic parameters were validated by comparing the near-surface soil moisture simulated by their coupled model and observed near-surface soil moisture data derived from a truck-mounted passive microwave radiometer. *Chang and Islam* [2000] also used artificial neural networks to estimate near-surface textural characteristics of the soil surface. Note, however, that the proper determination of soil hydraulic parameters in the unsaturated zone is vital for modeling profile soil moisture dynamics since they significantly affect the partitioning of the water balance, and hence the surface energy budget [*Xevi et al.*, 1996; *Antonopoulos*, 2000]. *Feddes et al.* [1993a, 1993b] postulated that regional inverse modeling could be feasible to derive vadose zone effective soil hydraulic parameters using evapotranspiration (ET) and surface soil moisture from remote sensing.

[5] In this paper, we present a near-surface soil moisture assimilation scheme for quantifying effective soil hydraulic properties of the vadose zone. First, we opted to conduct numerical experiments at the field scale to account for various hydrologic scenarios that may be encountered in the field, and to explore the strengths and limitations of the proposed method. Our numerical experiments generally aimed at addressing two major research questions: (1) Can we quantify effective soil hydraulic parameters of the root zone (0–100 cm) using only near-surface (0–5 cm) soil moisture data? (2) How robust are the derived soil hydraulic parameters, and can they closely describe the hydrologic processes in the subsurface soil layers? In our numerical experiments, we also present the effects of using evapo-

transpiration (ET) in tandem with near-surface soil moisture data as conditioning criteria for determining the effective soil hydraulic parameters. We also studied the combined effects of data and modeling errors in the parameter estimation. Then we applied the near-surface soil moisture assimilation scheme to a validation site within Little Washita watershed in Oklahoma to estimate the local-scale effective soil hydraulic properties. A major assumption of our study is that the flow in the soil system is considered to be primarily vertical. Hence the net surface run-on/runoff in the modeling domain is assumed to be zero approximating a flat land surface.

2. Materials and Methods

2.1. Near-Surface Soil Moisture Assimilation

2.1.1. Background

[6] Figure 1 shows a schematic of the near-surface soil moisture assimilation scheme. Here we used the near-surface soil moisture data θ(t) to determine θ(h) and K(h) functions simultaneously by tuning the soil hydrologic model using a genetic algorithm (see section 2.1.2). This approach is analogous to inverse modeling since it requires a physically based soil hydrologic model to run recursively until the solutions of θ(h) and K(h) have converged [e.g., *Kool and Parker*, 1988; *Van Dam et al.*, 1992, 1994; *Abbaspour et al.*, 1997; *Jhorar et al.*, 2002; *Ines and Droogers*, 2002]. The distinct feature of this approach is the type of conditioning criteria being used, which are derived from the near-surface soil layers (0–5 cm). This near-surface information is used to determine the effective soil hydraulic parameters for the entire root zone. Evidently, the success of this approach depends greatly on the assumption that a correlation between the near-surface and subsurface soil moisture exists, and thus any perturbations (e.g., those caused by plant activities) occurring in the soil surface could propagate downward, influencing the hydrologic processes underneath. Exploiting this dependency between the near-surface and subsurface processes would allow the determination of soil hydraulic properties in the root zone [*Abbaspour et al.*, 2001; *Ines and Droogers*, 2002]. This so-called codependency is the fundamental assumption used in near-surface data assimilation studies [e.g., *Walker et al.*, 2001]. The questions are as follows: (1) How far do the signatures of near-surface soil hydrologic processes propagate into the soil profile? (2) Will the assumption still hold if the processes in the subsurface layers are predominantly governed by the bottom boundary condition, e.g., by major upward fluxes from a shallow water table?

[7] The inverse problem of unsaturated flows in the vadose zone can be defined simply as estimating the soil hydrologic parameters **k** (equation (1)) by solving the physically based soil water flow equation (Richards equation) conditioned on a given time series of soil moisture data $\hat{\theta}_i$(t) derived from in situ measurements or from remote sensing observations (equation (2)) [*Kool and Parker*, 1988; *Van Dam et al.*, 1992, 1994; *Feddes et al.*, 1993a, 1993b]:

$$\mathbf{k} = \left\{ \mathbf{p}_{j=1,m} \right\} \tag{1}$$

$$\text{Minimize}\{Z(k)\} = \frac{1}{N}\frac{1}{M}\sum_{t=1}^{N}\sum_{i=1}^{M}\left|\theta_i(\mathbf{k},t) - \hat{\theta}_i(t)\right|. \tag{2}$$

[8] For our near-surface soil moisture assimilation studies, $\hat{\theta}_i$(t) corresponds to the near-surface soil moisture data and θ_i(**k**, t) corresponds to the simulated near-surface soil moisture given **k**, where Z is the objective function, N is the time domain, M is the number of soil layers considered in the soil profile, j is an index of parameter position, m is the maximum number of parameters, **p** corresponds to the soil hydraulic parameters, e.g., the Mualem-Van Genuchten parameters [*Mualem*, 1976; *Van Genuchten*, 1980], and i and t are running indices for soil layers and time.

[9] If other information is available e.g., ET data, equation (2) can be expanded as a weighted multicriteria function (equation (3a)), where f and (1 – f) are the weights associated with soil moisture and ET, respectively, ET(**k**, t) corresponds to the simulated ET given **k**, and $\hat{E}$T(t) corresponds to the observed evapotranspiration at time t. The weights f and (1 – f) signify the importance of near-surface soil moisture and ET during the parameter estimation. These weights can be assigned probabilistically or by a priori information based on field observation of (vertical) soil heterogeneity. Equation (3a) can be further extended into a θ and T (transpiration)-based function (equation (3b)) that could account for the contributions of soil moistures and root water extractions from different soil layers to the soil hydraulic parameter estimation [see *Feddes et al.*, 1993a; *Kabat et al.*, 1997; *Jhorar et al.*, 2002; *Ines and Droogers*, 2002]. Note that when including more than one conditioning variable (e.g., θ, ET, T) in equations (3a) and (3b), normalized variables instead of actual values are used to account for unit differences.

$$\text{Minimize}\{Z(\mathbf{k})\} = f\left\{\frac{1}{N}\frac{1}{M}\sum_{t=1}^{N}\sum_{i=1}^{M}\left|\theta_i(\mathbf{k},t) - \hat{\theta}_i(t)\right|\right\} + (1-f) \cdot \left\{\frac{1}{N}\sum_{t=1}^{N}\left|ET(\mathbf{k},t) - \hat{E}T(t)\right|\right\} \tag{3a}$$

$$\text{Minimize}\{Z(\mathbf{k})\} = f\left\{\frac{1}{N}\frac{1}{M}\sum_{t=1}^{N}\sum_{i=1}^{M}\left|\theta_i(\mathbf{k},t) - \hat{\theta}_i(t)\right|\right\} + (1-f) \cdot \left\{\frac{1}{N}\frac{1}{M}\sum_{t=1}^{N}\sum_{i=1}^{M}\left|T_1(\mathbf{k},t) - \hat{T}_i(t)\right|\right\} \tag{3b}$$

[10] The overall success of this approach lies on the robustness of the derived soil hydraulic parameters. Robust search algorithms, not easily trapped to local solutions, are a prerequisite for its successful implementation. In the following sections we discuss the search algorithm, hydrologic model, and parameter uncertainty analysis used in this study.

2.1.2. Genetic Algorithms

[11] Genetic algorithms (GAs) have been applied to solve complex problems in water resources systems [e.g., *Wang*, 1991; *Cieniawski et al.*, 1995; *Ritzel at al.*, 1994; *Oliveira and Loucks*, 1997; *Wardlaw and Sharif*, 1999; *Chan-Hilton and Culver*, 2000; *Wu et al.*, 2006] and to unsaturated flows in porous media [e.g., *Gwo*, 2001; *Vrugt et al.*, 2001; *Ines and Droogers*, 2002]. A comprehensive review of GA applications in hydrologic sciences is given by *Savic and Khu* [2005]. For completeness we briefly describe the

Table 1. Representations of the Mualem-Van Genuchten Parameters in the Genetic Algorithm[a]

Parameter	Search Space		Number of Bits (L)	2^L
	Minimum Values	Maximum Values		
α	0.0060	0.0330	5	32
n	1.200	1.610	6	64
θ_{res}	0.061	0.163	7	128
θ_{sat}	0.37	0.55	5	32
K_{sat}	1.84	55.7	10	1024

[a]Global search space = 32 × 64 × 128 × 32 × 1024 = 8,589,934,592. Example of $\mathbf{k} = \{\alpha, n, \theta_{res}, \theta_{sat}, K_{sat}\}$ = {00101 110010 0001111 00001 0101000101}. Probability of crossover = 0.5. Probability of creep mutation = 0.5. Probability of intermittent jump mutation = 0.05. Population = 10 chromosomes. Number of multipopulations = 3. Maximum generation = 500.

algorithm in this section. GAs are powerful search techniques that combine the survival of the fittest mechanism within a structured yet randomized information exchange to search for the solutions of complex search/optimization problems [*Holland*, 1975; *Goldberg*, 1989]. In binary GAs, the search spaces of the unknown parameters, e.g., the soil hydraulic parameters, are discretized into finite lengths and then coded as sets of binary substrings assembled to form string structures called chromosomes. The arrangement of binary digits (i.e., 0 and 1) within a chromosome can be a possible solution to the search problem. The procedure starts by randomly generating a population of chromosomes used as starting search positions to the search surface. Since several chromosomes are included within a population, multiple starting positions are explored at the start of the search simultaneously. The chromosomes are individually evaluated to determine their suitability based on a prescribed fitness function, i.e., the search surface. Then they undergo the process of selection, crossover, and mutation. On the basis of their fitness, they compete to be selected, and mate and reproduce for the next generation. During selection, the fitter chromosomes survive and the weaker ones die. The selected chromosomes randomly mate to exchange genetic information through the process of crossover to produce their offspring. The resulting new chromosomes are subjected to mutation to infuse fresh genetic materials for the new generation and to restore certain genetic characteristics that were lost due to degeneracy. The processes of selection, crossover, and mutation are repeated for many generations until the best possible solution is achieved; this solution is the fittest chromosome that evolved after many generations (see Figure 1). Detailed descriptions of GA can are given by *Goldberg* [1989] and *Michalewicz* [1996].

[12] In this study, we used a modified-microGA [*Ines and Droogers*, 2002] (see also D. L. Carroll, http://www.cuaerospace.com/carroll/ga.html) to solve for the unknown parameter set (Figure 1). A microGA uses a micropopulation to search for the search-surface. A unique feature of a microGA is that the micropopulation restarts when the majority of the chromosomes are similar in structure before the maximum generation is reached. Jump mutation (i.e., mutation at the binary level) is not allowed in a classic microGA [*Krishnakumar*, 1989]. Apparently, the microGA framework is highly suitable for coupled methodologies because of the lesser number of chromosomes involved during fitness evaluation, saving computational time. The restarting of the micropopulation mechanism also increases the resampling of the global search space with only a small number of parameter combinations being evaluated. Nevertheless, with the ill-posed nature of inverse problems [*Kool and Parker*, 1988], a restarting microGA can easily fall short of the elusive solution of the inverse problem. Besides, the new chromosomes from the restarted population are raw combinations of parameters not conditioned on the converging parameter search spaces. D. L. Carroll (http://www.cuaerospace.com/carroll/ga.html) introduced a creep mutation operator in a microGA to infuse new genetic materials to the restarting micropopulation, which resulted in an improved performance of the microGA. A creep mutation is a mutation variant that alters the parameter set $\mathbf{k}$ at the decimal level, thus minimizing the perturbations made on the converging parameter combinations. This minimized parameter perturbation does not compromise the micropopulation restarting mechanism in a microGA. *Ines and Droogers* [2002] further modified the algorithm to enhance more the potential benefits of a restarting micropopulation for inverse modeling of unsaturated flows.

[13] Moreover, we added several new features to the modified microGA for this study. We implemented a first-order time-saving scheme where the chromosomes in the previous generation (g-1) are remembered and compared with the present generation (g) to evaluate if similar chromosomes exist such that they can directly inherit the properties of the former, reducing further the computational time [*Ines and Honda*, 2005]. A new feature called intermittent jump mutation was introduced at selected instances along the generations (e.g., 25th, 50th, 75th, and 85th percentile of the maximum generation) to introduce further fresh influx of new genetic material to the converging micropopulation. In the GA search, we used a binary tournament selection process, a uniform crossover to exchange genetic information between the selected chromosomes, a micropopulation of 10, and a maximum number of generations of 500 (see Table 1).

[14] For the inverse-modeling-based near-surface soil moisture assimilation, we considered the soil hydraulic parameters of the Mualem–Van Genuchten functions as unknowns expressed as $\mathbf{k} = \{\alpha, n, \theta_{res}, \theta_{sat}, K_{sat}, \lambda\}$. Since λ is assumed to be 0.5 (*Mualem* [1976]; see section 2.1.3) and defining $\mathbf{p}_{j=1,\,m-1} = \{\alpha, n, \theta_{res}, \theta_{sat}, K_{sat}\}$ (see equation (1)), hence $\mathbf{k} = \{\mathbf{p}_{j=1,\,m-1}, \lambda\}$ (see section 2.1.3 for parameter definitions). The parameters $\mathbf{p}'(\mathbf{p}_{j=1,\,m-1})$ were the only ones propagated in GA, and their binary and decimal representations are given in Table 1. The maximum ranges of the parameter values were designed to accommodate a variety of soils ranging from clay to sandy loam [*Leij et al.*, 1999]. The fitness function was defined as

$$\text{fitness}(\mathbf{p}') = \frac{1}{Z(\mathbf{k})}, \tag{4}$$

where the binary elements of $\mathbf{p}'$ are concatenated with their decimal values using the linear mapping technique of *Goldberg* [1989]:

$$C\left(p_j\right) = C_{Min}\left(p_j\right) + \frac{\sum_{h=1}^{Lp_j} a_h 2^{h-1}}{2^{L_{p_j}} - 1}\left[C_{Max}\left(p_j\right) - C_{Min}\left(p_j\right)\right] \forall j, \tag{5}$$

where C_{Max} and C_{Min} correspond to the maximum range of parameter p (elements of $\mathbf{p}'$); C is the decimal value of a binary substring p; L_p is the length of the substring p; a is the bit value 0 or 1 at position h in the substring; and j is an index for parameter position in the string $\mathbf{p}'$.

2.1.3. Simulation Model

[15] SWAP [*Van Dam et al.*, 1997] is a variably saturated flow model used to simulate the processes of the soil-water-atmosphere-plant system. It solves the one-dimensional Richards equation (equation (6)) using a robust implicit finite difference scheme [*Belmans et al.*, 1983] to simulate soil moisture dynamics in the soil profile under different climatic and environmental conditions,

$$\frac{\partial\theta(\mathrm{h})}{\partial \mathrm{t}} = C(\mathrm{h})\frac{\partial \mathrm{h}}{\partial \mathrm{t}} = \frac{\partial\left[\mathrm{K}(\mathrm{h})\left(\frac{\partial \mathrm{h}}{\partial \mathrm{z}}+1\right)\right]}{\partial \mathrm{z}} - \mathrm{S}(\mathrm{h}), \tag{6}$$

where θ is the soil moisture ($cm^3\ cm^{-3}$), K is the hydraulic conductivity ($cm\ d^{-1}$), h is the soil water pressure head (per cm), z is the soil depth (cm) taken positively upward, t is time (d), C is the differential water capacity (cm^{-1}), and S(h) is the actual soil moisture extraction rate by plants ($cm^3\ cm^{-3}\ d^{-1}$) defined as equation (7) in case of a uniform root distribution

$$\mathrm{S}(\mathrm{h}) = \alpha_{\mathrm{w}}(\mathrm{h})\frac{\mathrm{T}_{\mathrm{pot}}}{|\mathrm{z}_{\mathrm{r}}|}, \tag{7}$$

where T_{pot} is the potential transpiration ($cm\ d^{-1}$), z_r the rooting depth (cm), and α_w is a reduction factor as function of h and accounts for water deficit and oxygen stress [*Feddes et al.*, 1978]. SWAP can simulate many configurations of the root density.

[16] The soil hydraulic functions in SWAP are defined by the Mualem-Van Genucthen equations [*Van Genuchten*, 1980; *Mualem*, 1976]

$$\mathrm{S}_{\mathrm{e}} = \frac{\theta(\mathrm{h})-\theta_{\mathrm{res}}}{\theta_{\mathrm{sat}}-\theta_{\mathrm{res}}} = \left[\frac{1}{1+|\alpha \mathrm{h}|^{\mathrm{n}}}\right]^{\mathrm{m}} \tag{8}$$

$$\mathrm{K}(\mathrm{h}) = \mathrm{K}_{\mathrm{sat}}\mathrm{S}_{\mathrm{e}}^{\lambda}\left[1-\left(1-\mathrm{S}_{\mathrm{e}}^{1/\mathrm{m}}\right)^{\mathrm{m}}\right]^2, \tag{9}$$

where S_e is the relative saturation(), α (cm^{-1}) is a shape parameter equivalent to the inverse of the bubbling pressure, n() is a shape parameter that accounts for the pore size distribution, θ_{res} ($cm^3\ cm^{-3}$) and θ_{sat} ($cm^3\ cm^{-3}$) are the residual and saturated soil moisture content respectively, K_{sat} ($cm\ d^{-1}$) is the saturated hydraulic conductivity, and λ() is a shape parameter that accounts for tortuosity in the soil. *Van Genuchten* [1980] proposed m = 1 – 1/n. The values of these parameters are distinct among soil textural types and have to be defined as inputs to the simulation model. *Mualem* [1976] suggested a representative value of λ equal to 0.5 for most soils, although this value may not be optimal in many situations [*Schaap and Leij*, 2000].

[17] SWAP accounts for several combinations of the top and bottom boundary conditions (e.g., Dirichlet, Neumann, and Cauchy types). It is equipped with crop growth models and water management modules for irrigation and drainage studies. The model simulates both soil water quantity and quality with a temporal resolution of 1 day.

[18] The potential evapotranspiration (ET_{pot}) is calculated by SWAP using the Penman-Monteith equation, where the components potential transpiration (T_{pot}) and soil evaporation (E_{pot}) are partitioned using the leaf area index (LAI) or soil cover fraction (SC) of the simulated land unit. As the soil dries, SWAP reduces ET_{pot} into actual ET (ET_{act}) using the adjusted values of E_{pot} and T_{pot} into actual values based on the existing environmental conditions calculated from established empirical relationships. The model has been well validated in the field and found to perform very well under different climatic and environmental conditions [e.g., *Wesseling and Kroes*, 1998; *Sarwar et al.*, 2000; *Droogers et al.*, 2000, *Singh et al.*, 2006a, 2006b]. In this study, we used SWAP as our soil hydrologic model to evaluate the parameter set $\mathbf{p}'$ proposed by GA (recall that $\mathbf{k} = \{\mathbf{p}', \lambda\}$; see section 2.1.2). Detailed descriptions of SWAP are given by *Van Dam et al.* [1997] and *Van Dam* [2000].

2.1.4. Parameter Uncertainty

[19] To quantify the parameter uncertainty, we used a technique that may allow a microGA to provide some estimates of the uncertainty levels. Although GA is a stochastic approach and contains a population of possible solutions in a generation, it is inherently limited to account for the uncertainty of the solution since we consider a solution in a GA as the best chromosome of the population. One might argue that we can use the whole population for estimating parameter uncertainties. In the case of a simple GA [see *Goldberg*, 1989], this may not be adequate because the weaker chromosomes are not considered solutions to the problem. Also, in this study, when a microGA converges, most of the chromosomes are almost alike. This problem is exacerbated by the elitist, non-niching nature of a microGA as it tries to converge only to one region (near-optimal/optimal) in the search surface. For this reason, we chose to use a multipopulation search in an attempt to estimate parameter uncertainties under the perfect model/data condition scenarios. This may give us also an opportunity to estimate nonuniqueness in the solutions, as this step is analogous to solving the inverse problem from multiple different starting positions on the search surface. Multipopulated GAs have been used for hydrologic modeling before but not with the intent of estimating for uncertainty in parameter estimates [*Seibert*, 2000]. In this study, by using three micropopulations running in parallel, we searched the search surface for the inverse modeling solutions (see Table 1 for the ranges of parameter search spaces). At the end of the maximum generation, the successful chromosomes from the multipopulations were integrated together and then classified as above-averaged if their fitness exceeds the grand average fitness defined by the average of all the chromosome fitness from the multipopulation or below-averaged, otherwise. The above-averaged chromosomes are considered to be the most probable solutions of GA to the inverse problem and were used for estimating uncertainties of the parameter estimates (see Figure 1), while the below-averaged chromosomes are discarded from the final solution. The uncertainty of parameter estimates was estimated by calculating the 95%

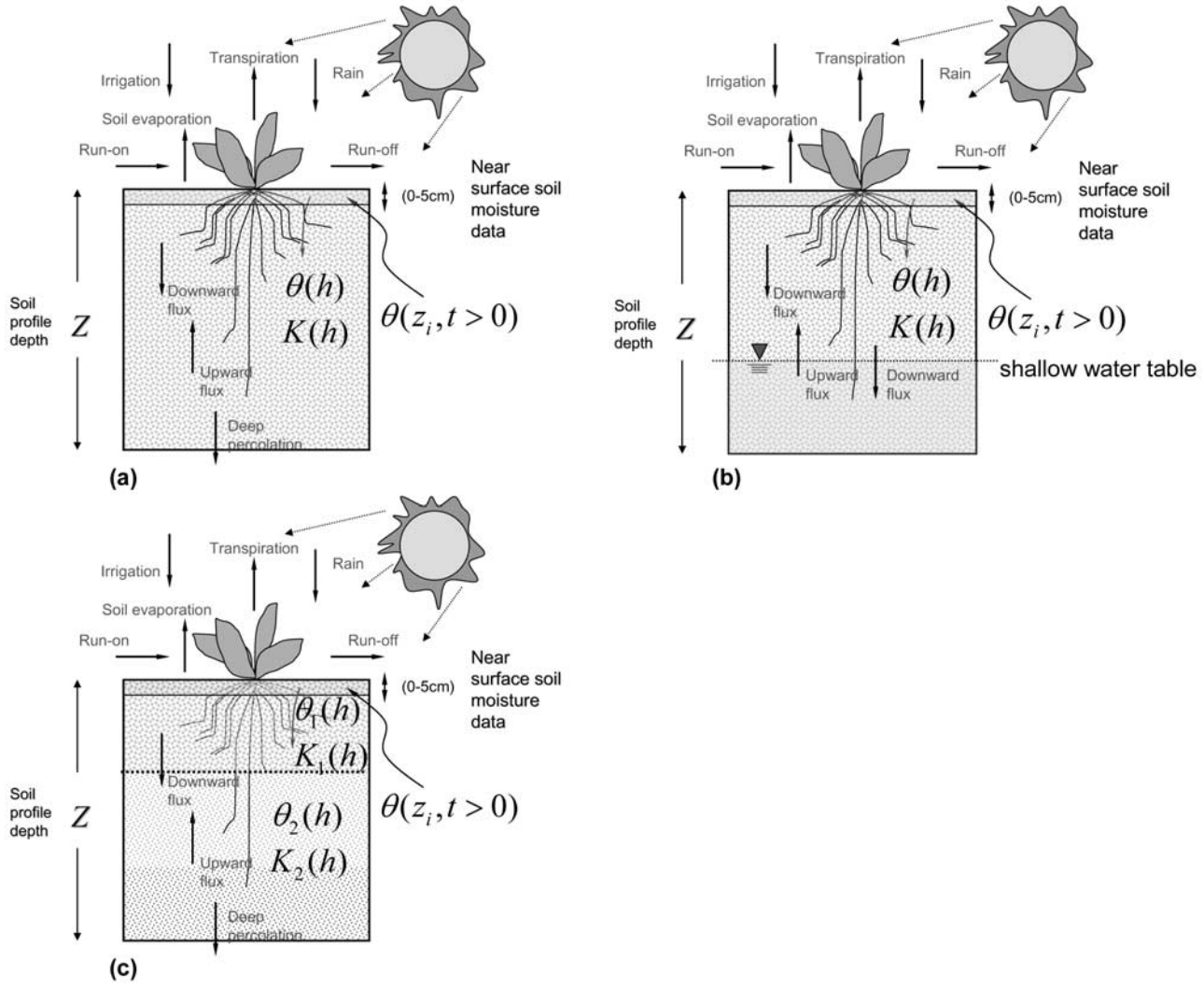

Figure 2. Schematic layout of the model domain and flow conditions used in the numerical experiments: (a) homogenous soil column under a free-draining condition; (b) homogenous soil column with shallow water table; and (c) heterogeneous soil column under a free-drainage condition.

confidence interval (95PCI) of the derived parameter values. The uniqueness of the solutions were estimated using equation (10),

$$\text{Range}_{ijk} = 95\text{PCI}_{ijk+} - 95\text{PCI}_{ijk-} \; \forall i, \forall j, \forall k, \qquad (10)$$

where 95PCI_{ijk+} and 95PCI_{ijk-} indicate the upper and lower bounds, respectively, of the 95PCI; i, j, and k are indices for hydrologic year, soil hydraulic parameter, and soil type, respectively. For a high degree of uniqueness, equation (10) should yield a near-zero value. It should be noted that this parameter uncertainty estimation as used in this paper is an attempt to deal with uncertainties in GAs and should not be viewed as a finished project, but rather as an ad hoc scheme that can possibly be improved in future.

[20] In real-world conditions, aside from the skill of the search algorithm, other factors like model imperfections, data and modeling errors, and the ill-posed nature of the inverse problem all contribute to uncertainties of the parameter estimates [see *Kool et al.*, 1987; *Kool and Parker*, 1988; *Russo et al.*, 1991; *Van Dam et al.*, 1992; *Šimůnek et al.*, 1998; *Romano and Santini*, 1999]. For this reason, we also made some parameter estimation experiments under uncertainty considering an imperfect data and/or modeling conditions (see section 2.2.2.4).

2.2. Numerical Experiments

2.2.1. Model Domain and Flow Conditions

[21] This study was conducted as a proof of concept that the effective soil hydraulic parameters of the soil profile can be quantified using near-surface soil moisture data such as those measured from remote sensing. Hence we opted to use numerical experiments of unsaturated flows to cover a wide range of hydrologic conditions (Figure 2) that will test most of the questions posed in the previous sections. As with any numerical experiments [e.g., *Kool and Parker*, 1988; *Walker et al.*, 2001; *Walker and Houser*, 2004], we generated hypothetical soil moisture data from available soils, weather, and crop management information from the study site. We considered three typical hydrologic years of varying rainfall patterns: dry, relatively wet, and wet years based on climatology in northern Texas (see Figure 3; http://mesonet.

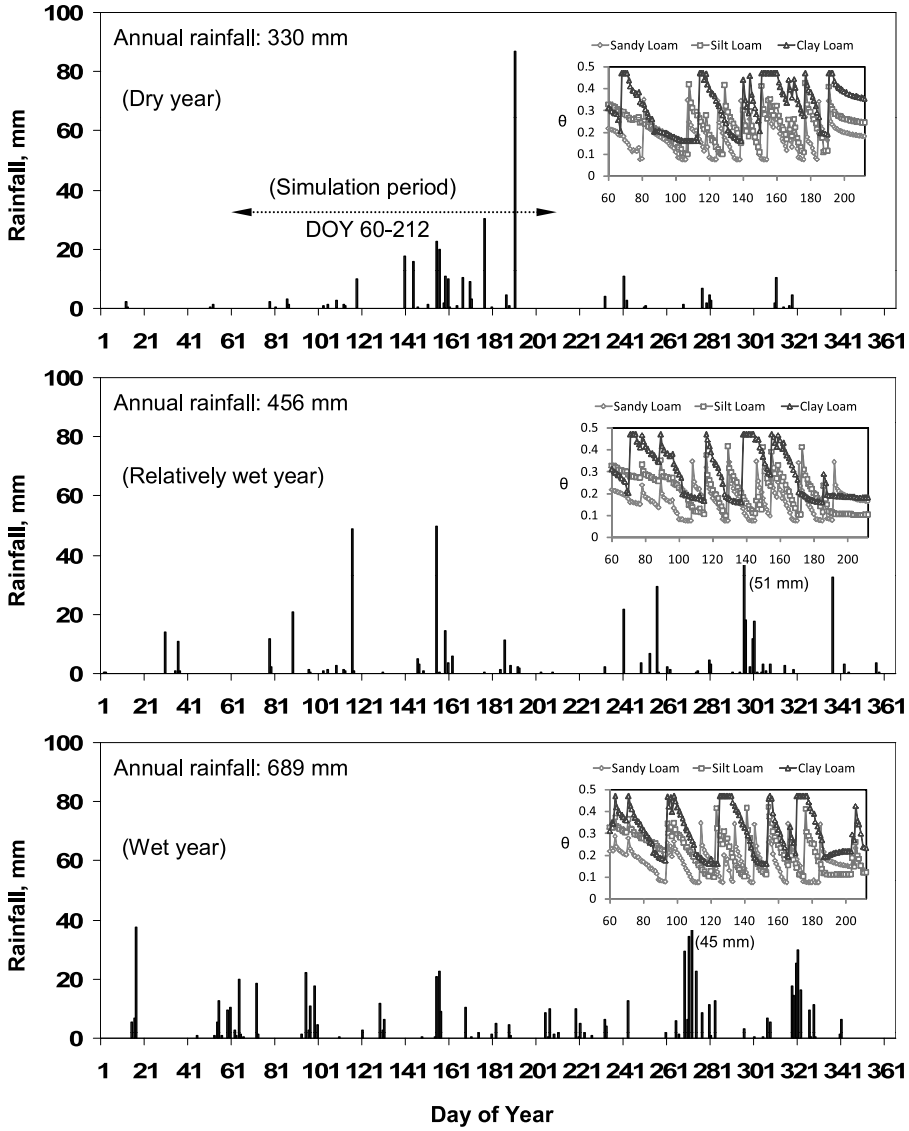

Figure 3. Rainfall patterns used in the numerical experiments under northern Texas climate. Insets show near-surface soil moisture patterns used in the parameter estimation.

tamu.edu/). A land unit with a soil depth of 200 cm and a ponding depth of 10 cm was considered for simulations. The crop considered was wheat (*Triticum aestivum*) under irrigated condition. Under the base scenario, irrigation was applied by SWAP automatically according to an irrigation scheduling criterion based on allowable water stress by the crops (here $T_{act}/T_{pot} \geq 0.70$; see section 2.1.3 for definitions). If this crop water stress level is exceeded, SWAP applies 100 mm of water by surface irrigation. Three different soil types were considered in the simulations. i.e., (1) sandy loam, (2) silt loam, and (3) clay loam representing a wide range of soils for this numerical study (UNSODA database [*Leij et al.*, 1999]). The expected values of the Mualem-Van Genuchten soil hydraulic parameters for sandy loam, silt loam, and clay loam soils are given in Tables 2a, 2b, and 2c (based on UNSODA). Other meteorological data including daily solar radiation, wind speed, maximum and minimum air temperature, and humidity used in this study were collected from the Texas Mesonet station in Lubbock, Texas (http://mesonet.tamu.edu/). All SWAP simulations were done across the crop growing season from 1 March to 31 July (days of year (DOY) 60–212) for all the years considered in the numerical experiments.

2.2.2. Numerical Case Studies

2.2.2.1. Case 1: Homogenous Free-Draining Column

[22] The first case study involves a homogenous free-draining column (Figure 2a), a scenario representing deep draining soils like soils in arid/semiarid regions. The soil column was discretized into 33 computational layers with finer divisions from the soil surface to a depth of 10 cm. For all the simulations, the soil columns were initialized uniformly at −100 cm pressure head (h) (i.e., initial profile soil moisture contents are calculated at this initial pressure head distribution). The near-surface soil moisture assimilation procedure was conducted using various data collection/aggregation schemes including a (1) daily interval protocol (D), (2) weekly interval (W), (3) 7-day average (7D), and (4) a wet/dry window scheme (WDW) to explore the best possible data collection/aggregation scheme for the parameter estimation. The WDW scheme is implemented by

Table 2a. Solutions of the Genetic Algorithm to the Near-Surface Soil Moisture Assimilation Under Sandy Loam Soil, Case 1, Homogenous, Free-Draining Column

			Dry Year		Relatively Wet Year		Wet Year	
Parameter	Expected Value[a]	Collection Scheme	Mean	95PCI	Mean	95PCI	Mean	95PCI
α	0.021	daily interval	0.022	0.020–0.023	0.022	0.020–0.023	0.022	0.021–0.024
		weekly interval	0.022	0.020–0.024	0.022	0.020–0.023	0.022	0.021–0.024
		7-day average	0.022	0.020–0.024	0.023	0.021–0.024	0.022	0.020–0.024
		wet/dry window	0.022	0.021–0.023	0.022	0.021–0.024	0.022	0.020–0.023
n	1.61	daily interval	1.61	1.60–1.61	1.61	1.60–1.62	1.61	1.59–1.62
		weekly interval	1.61	1.61–1.61	1.60	1.57–1.63	1.61	1.60–1.61
		7-day average	1.61	1.59–1.62	1.61	1.61–1.61	1.61	1.60–1.62
		wet/dry window	1.61	1.60–1.61	1.61	1.61–1.61	1.61	1.60–1.61
θ_{res}	0.067	daily interval	0.066	0.064–0.068	0.066	0.064–0.068	0.068	0.065–0.071
		weekly interval	0.067	0.065–0.068	0.066	0.064–0.068	0.067	0.067–0.067
		7-day average	0.067	0.065–0.068	0.066	0.063–0.069	0.067	0.066–0.068
		wet/dry window	0.067	0.066–0.068	0.067	0.067–0.067	0.067	0.067–0.067
θ_{sat}	0.370	daily interval	0.372	0.366–0.378	0.374	0.366–0.382	0.374	0.365–0.383
		weekly interval	0.373	0.367–0.380	0.374	0.367–0.380	0.378	0.372–0.385
		7-day average	0.375	0.369–0.380	0.380	0.366–0.394	0.378	0.366–0.389
		wet/dry window	0.375	0.366–0.383	0.377	0.367–0.387	0.374	0.363–0.384
K_{sat}	41.6	daily interval	44.1	37.0–51.1	45.3	37.3–53.3	48.1	39.6–56.5
		weekly interval	44.4	38.0–50.8	46.5	35.9–57.0	50.4	41.1–59.7
		7-day average	46.1	37.3–55.0	50.6	38.8–62.3	48.9	37.8–59.9
		wet/dry window	46.0	37.6–54.5	48.7	38.3–59.1	45.1	35.0–55.3

[a]UNSODA database [*Leij et al.*, 1999].

passing a moving window across the time series of near-surface soil moisture and aggregating soil moisture data during drying and wetting periods. Among the four data collection/aggregation schemes, the WDW is based more on the physics of the soil water movement because the daily soil moisture data were aggregated based on a wetting event and subsequent drying phases. All experiments have three replicates by using multiple populations in the GA implementations (see section 2.1.4). For case 1, a total of 108 numerical simulations were conducted, i.e., 3 soil types $\times$ 3 years (see Figure 3) $\times$ 4 data collection schemes $\times$ 3 replicates.

2.2.2.2. Case 2: Homogenous Column With a Shallow Water Table

[23] The second case represents soils with shallow water table for all year-round (Figure 2b). At the onset of simulations, the initial pressure heads of the soil column were in equilibrium with the shallow water table, at 150 cm deep from the soil surface. The bottom flux (positive upward) is calculated using $h(z = -150, t > 0) = 0$ cm

Table 2b. Solutions of the Genetic Algorithm to the Near-Surface Soil Moisture Assimilation Under Silt Loam Soil, Case 1, Homogenous, Free-Draining Column

			Dry Year		Relatively Wet Year		Wet Year	
Parameter	Expected Value[a]	Collection Scheme	Mean	95PCI	Mean	95PCI	Mean	95PCI
α	0.012	daily interval	0.011	0.009–0.013	0.013	0.011–0.016	0.013	0.008–0.018
		weekly interval	0.011	0.010–0.012	0.011	0.010–0.013	0.013	0.007–0.018
		7-day average	0.010	0.009–0.011	0.013	0.010–0.017	0.011	0.010–0.012
		wet/dry window	0.011	0.010–0.013	0.014	0.011–0.016	0.013	0.011–0.014
n	1.39	daily interval	1.44	1.32–1.56	1.39	1.37–1.40	1.39	1.37–1.41
		weekly interval	1.52	1.41–1.63	1.41	1.39–1.42	1.41	1.34–1.48
		7-day average	1.51	1.38–1.65	1.44	1.39–1.49	1.43	1.38–1.47
		wet/dry window	1.40	1.36–1.45	1.38	1.34–1.42	1.39	1.37–1.40
θ_{res}	0.061	daily interval	0.078	0.045–0.110	0.062	0.060–0.063	0.062	0.061–0.064
		weekly interval	0.101	0.073–0.128	0.065	0.062–0.067	0.066	0.056–0.075
		7-day average	0.090	0.058–0.123	0.069	0.059–0.079	0.065	0.057–0.073
		wet/dry window	0.067	0.049–0.085	0.063	0.059–0.067	0.062	0.061–0.063
θ_{sat}	0.430	daily interval	0.435	0.409–0.462	0.441	0.422–0.459	0.440	0.417–0.462
		weekly interval	0.447	0.423–0.472	0.428	0.415–0.441	0.440	0.420–0.461
		7-day average	0.442	0.421–0.463	0.460	0.426–0.495	0.435	0.422–0.449
		wet/dry window	0.431	0.422–0.440	0.437	0.429–0.445	0.439	0.429–0.449
K_{sat}	30.5	daily interval	29.7	22.0–37.4	41.6	24.8–58.3	41.6	15.5–67.7
		weekly interval	31.1	25.1–37.0	26.6	20.2–33.0	39.3	6.8–71.7
		7-day average	24.3	17.8–30.7	43.9	23.4–64.5	27.0	22.6–31.4
		wet/dry window	30.3	23.7–36.8	41.0	27.7–54.3	40.8	27.3–54.2

[a]UNSODA database [*Leij et al.*, 1999].

Table 2c. Solutions of the Genetic Algorithm to the Near-Surface Soil Moisture Assimilation Under Clay Loam Soil, Case 1, Homogenous, Free-Draining Column

Parameter	Expected Value[a]	Collection Scheme	Dry Year		Relatively Wet Year		Wet Year	
			Mean	95PCI	Mean	95PCI	Mean	95PCI
α	0.030	daily interval	0.030	0.028–0.031	0.030	0.027–0.032	0.030	0.027–0.032
		weekly interval	0.029	0.026–0.032	0.030	0.029–0.032	0.030	0.028–0.031
		7-day average	0.030	0.029–0.031	0.030	0.027–0.033	0.030	0.027–0.033
		wet/dry window	0.030	0.028–0.031	0.029	0.028–0.031	0.031	0.029–0.033
n	1.37	daily interval	1.38	1.34–1.41	1.40	1.37–1.44	1.38	1.36–1.41
		weekly interval	1.38	1.34–1.43	1.38	1.35–1.42	1.36	1.33–1.40
		7-day average	1.37	1.33–1.41	1.38	1.32–1.44	1.39	1.35–1.43
		wet/dry window	1.36	1.35–1.38	1.42	1.40–1.44	1.39	1.36–1.41
θ_{res}	0.129	daily interval	0.131	0.122–0.139	0.137	0.128–0.147	0.134	0.126–0.142
		weekly interval	0.135	0.123–0.148	0.132	0.121–0.144	0.126	0.116–0.136
		7-day average	0.127	0.115–0.139	0.130	0.118–0.142	0.135	0.122–0.148
		wet/dry window	0.128	0.123–0.133	0.141	0.138–0.143	0.133	0.124–0.141
θ_{sat}	0.470	daily interval	0.471	0.465–0.476	0.473	0.468–0.479	0.471	0.465–0.477
		weekly interval	0.471	0.465–0.476	0.472	0.465–0.478	0.470	0.465–0.475
		7-day average	0.471	0.465–0.478	0.472	0.465–0.478	0.472	0.466–0.479
		wet/dry window	0.469	0.469–0.469	0.476	0.472–0.481	0.473	0.468–0.479
K_{sat}	1.84	daily interval	1.87	1.82–1.93	1.88	1.80–1.96	1.87	1.81–1.92
		weekly interval	1.87	1.80–1.94	1.90	1.73–2.07	1.88	1.81–1.96
		7-day average	1.87	1.81–1.93	1.90	1.76–2.04	1.89	1.80–1.98
		wet/dry window	1.86	1.80–1.91	1.88	1.81–1.94	1.87	1.81–1.92

[a]UNSODA database [*Leij et al.*, 1999].

[*Van Dam*, 2000]. This case was conducted to test if the codependency assumption (see section 2.1.1) used in near-surface soil moisture assimilation studies [e.g., *Walker et al.*, 2001] is still valid if the flow processes in the unsaturated zone are dominated by the bottom boundary condition, e.g., by major upward flows from shallow water table. On the basis of our findings in case 1 (described later), we applied only the wet/dry window (WDW) data collection scheme for case 2, resulting in a total of 27 experiments, i.e., 3 soil types × 3 years × 3 replicates. An additional 54 experiments (27 for each additional groundwater table depths at 200 and 100 cm) were also conducted to assess the impacts of varying water table depths to the performance of the near-surface soil moisture assimilation procedure.

2.2.2.3. Case 3: Heterogeneous Column

[24] For case 3, the heterogeneous soil profile was composed of sandy loam (top 60 cm) and silt loam (bottom 140 cm) layers and was assumed to be well drained (Figure 2c). As in case 2, we applied only the WDW data collection scheme for case 3. For the two-layer system, the GA chromosome was defined as

$$\mathbf{p}_{j=1,m-2} = \{\alpha_1, n_1, \theta_{res1}, \theta_{sat1}, K_{sat1}, \alpha_2, n_2, \theta_{res2}, \theta_{sat2}, K_{sat2}\}$$

and thus

$$\mathbf{k} = \{\mathbf{p}'', \lambda_1, \lambda_2\},$$

where $\lambda_1 = \lambda_2 = 0.5$ and $\mathbf{p}''$ is $\mathbf{p}_{j\,=\,1,\,m-2}$. For all our numerical experiments under heterogeneous condition, we used a single-criterion procedure with near-surface soil moisture as conditioning variable (see equation (2)), and a multicriteria procedure using (f × (soil moisture) + (1 − f) × evapotranspiration (ET)) (see equation (3a)), where f is the weight given to the near-surface soil moisture and (1 − f) is the weight given to evapotranspiration. In equation (3a), the soil moisture and ET values were normalized, thus allowing

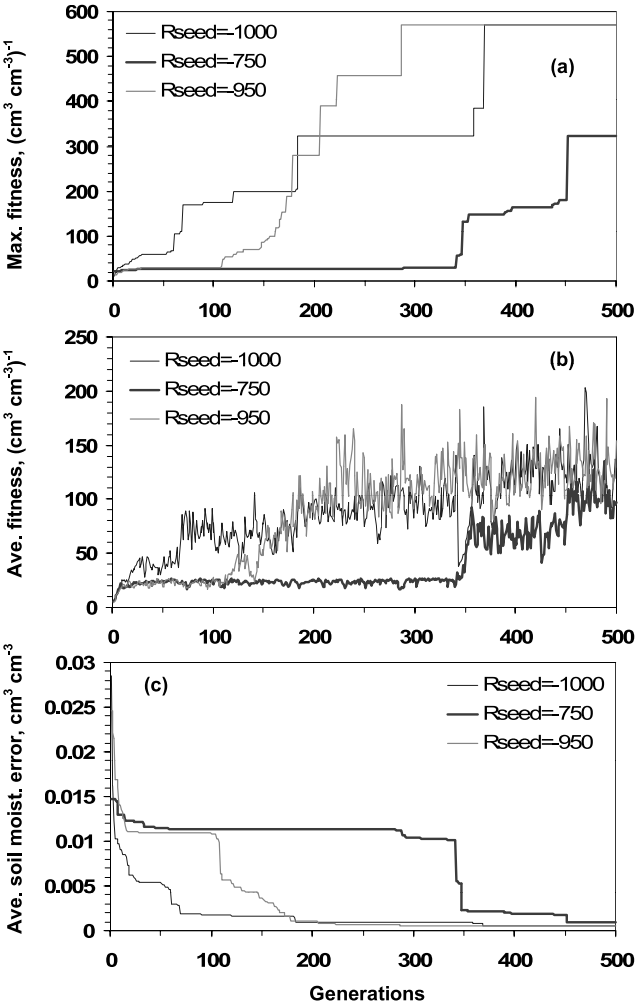

Figure 4. Example of a genetic algorithm solution: clay loam, dry year, wet/dry window (WDW) scheme: (a) maximum fitness, (b) average fitness, and (c) average soil moisture error (near surface).

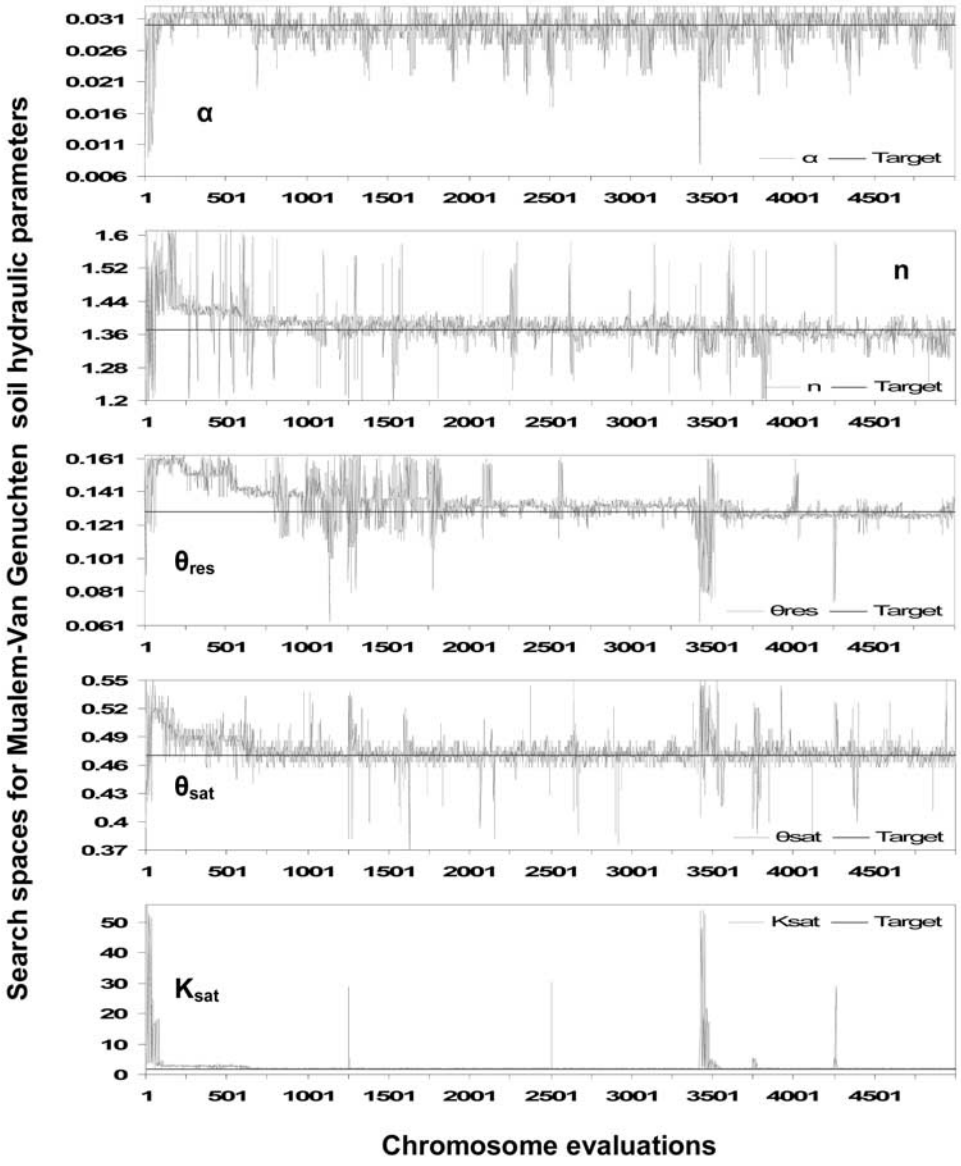

Figure 5. Chronological search space exploration of the search surface $\mathbf{Z} = f(\alpha, n, \theta_{res}, \theta_{sat}, K_{sat})$ bounded by $\alpha_{min} \leq \alpha \leq \alpha_{max}$, $n_{min} \leq n \leq n_{max}$, $\theta_{resmin} \leq \theta_{res} \leq \theta_{resmax}$, $\theta_{satmin} \leq \theta_{sat} \leq \theta_{satmax}$, and $K_{satmin} \leq K_{sat} \leq K_{satmax}$ (see Table 1). Case 1, clay loam; WDW scheme; seed = −1000; population size, 10; number of generations, 500; α (cm^{-1}); n, ( ); θ_{res} (cm^3 cm^{-3}); θ_{sat} (cm^3 cm^{-3}); K_{sat} (cm d^{-1}).

the use of both variables in one equation. ET was used as a secondary search criterion because in theory it could influence the perturbations at deeper soil layers due to its transpiration (T) component, and as a result it could impact parameter identifiability [e.g., *Feddes et al.*, 1993a, 1993b; *Jhorar et al.*, 2002; *Ines and Droogers*, 2002] of the silt loam layer underlain by the sandy loam layer (Figure 2c). In the experiments, four scenarios were considered based on the following conditioning criteria, using (1) soil moisture alone (f = 1.0), (2) soil moisture and ET with f = 0.6, (3) soil moisture and ET with f = 0.5, and (4) soil moisture and ET with f = 0.4, resulting in a total of 36 experiments, i.e., 4 conditioning criteria × 3 years × 3 replicates.

2.2.2.4. Parameter Estimation Under Uncertainty

[25] The case studies above assumed a perfect model and data conditions. Hence the uncertainties in the parameter estimates could be attributed to the search algorithm, including the form of the objective function; the information content of the data, which include the type, data variability, and their sensitivity to the soil hydraulic parameters; and to the ill-posed nature of inverse problems [e.g., *Kool et al.*, 1987; *Kool and Parker*, 1988; *Russo et al.*, 1991; *Van Dam et al.*, 1992, 1994; *Šimůnek et al.*, 1998; *Romano and Santini*, 1999; *Vrugt et al.*, 2001; *Ines and Droogers*, 2002]. In this part of the study, we only considered the effects of data and modeling errors on the performance of our near-surface soil moisture assimilation scheme. We used the sandy loam soil case under the dry year condition with homogenous free-draining column for our error analysis (case 1; see section 2.2.2.1). To account for data errors, we perturbed the "error-free" near-surface soil moisture data assuming that soil moisture errors are normally distributed using $\theta' = \theta \times (1 + x\xi)$ where $x \sim N(0, 1)$ and $-1 \leq x \leq 1$; θ'

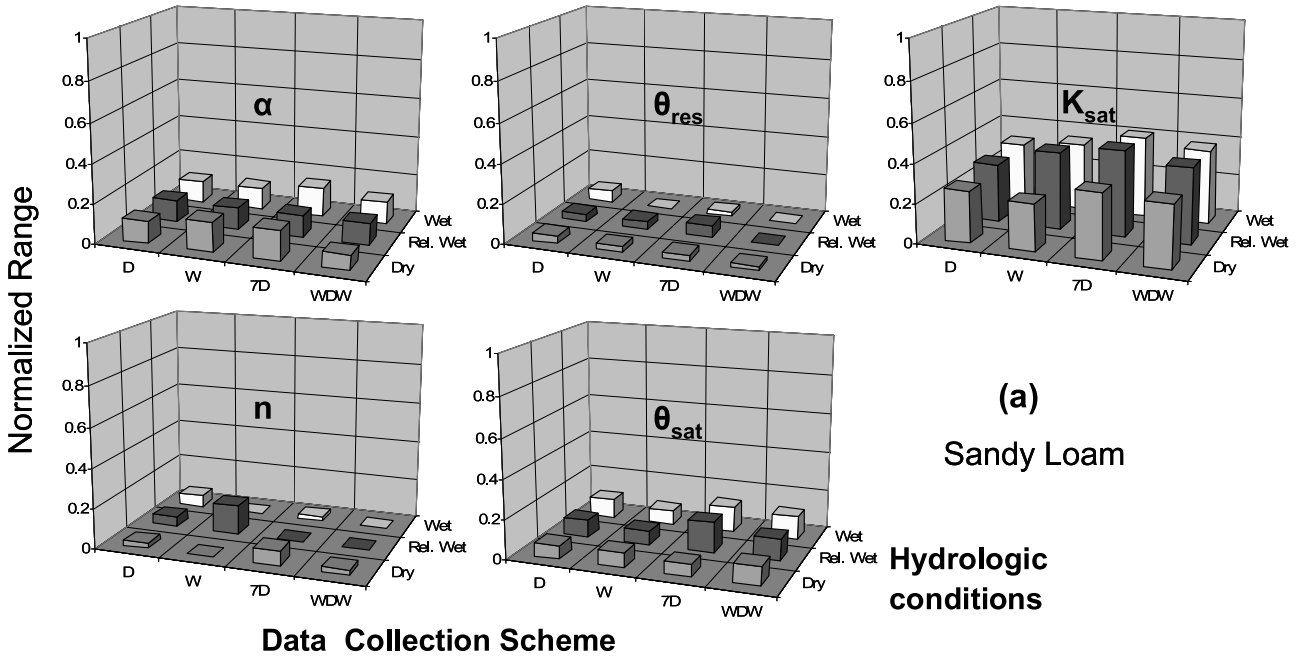

Figure 6a. Uniqueness of solutions for sandy loam for case 1 under free-draining condition. D, daily; W, weekly, 7D, 7-day average; WDW, wet/dry window. Values are normalized based on the minimum and maximum values of the parameters from Table 1.

and θ are the perturbed and error-free soil moisture, respectively; x is a normal random deviate with mean and standard deviation equal to 0 and 1, respectively; and ξ is the error term. An error of 20% was propagated along the time series of error-free near-surface soil moisture, in which 10 perturbed soil moisture series were generated. This ξ term can be associated with measurement errors that could be incurred during the field data collection. To account for modeling (structural) errors, we considered the effects of rooting depth and root density variation on the performance of the near-surface soil moisture assimilation scheme. Two root densities were studied, i.e., a triangular (0–1 m depth: 100–0.01% density) and a trapezoidal configuration (0–0.5–1.0 m depth: 100–100–0.01% density). The rooting depth scenarios include a condition in which the rooting depth was shallower than the base case scenario. In our base scenario, the potential

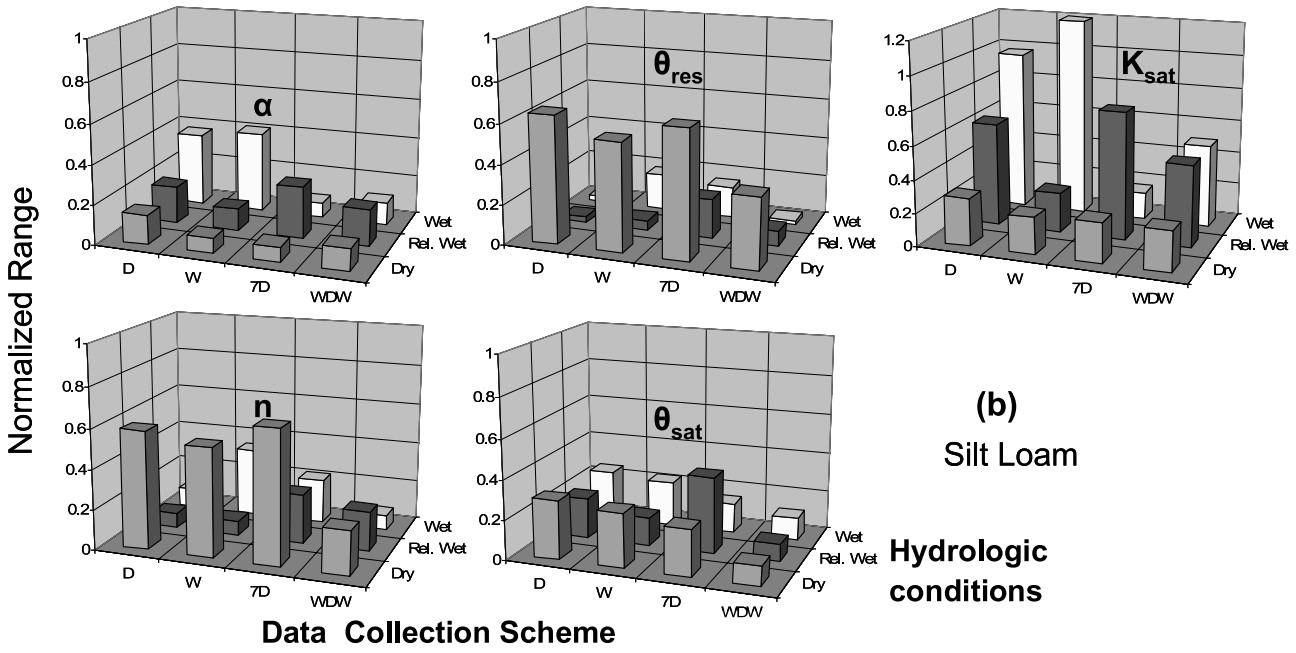

Figure 6b. Uniqueness of solutions for silt loam for case 1 under free-draining condition. D, daily; W, weekly, 7D, 7-day average; WDW, wet/dry window. Values are normalized based on the minimum and maximum values of the parameters from Table 1.

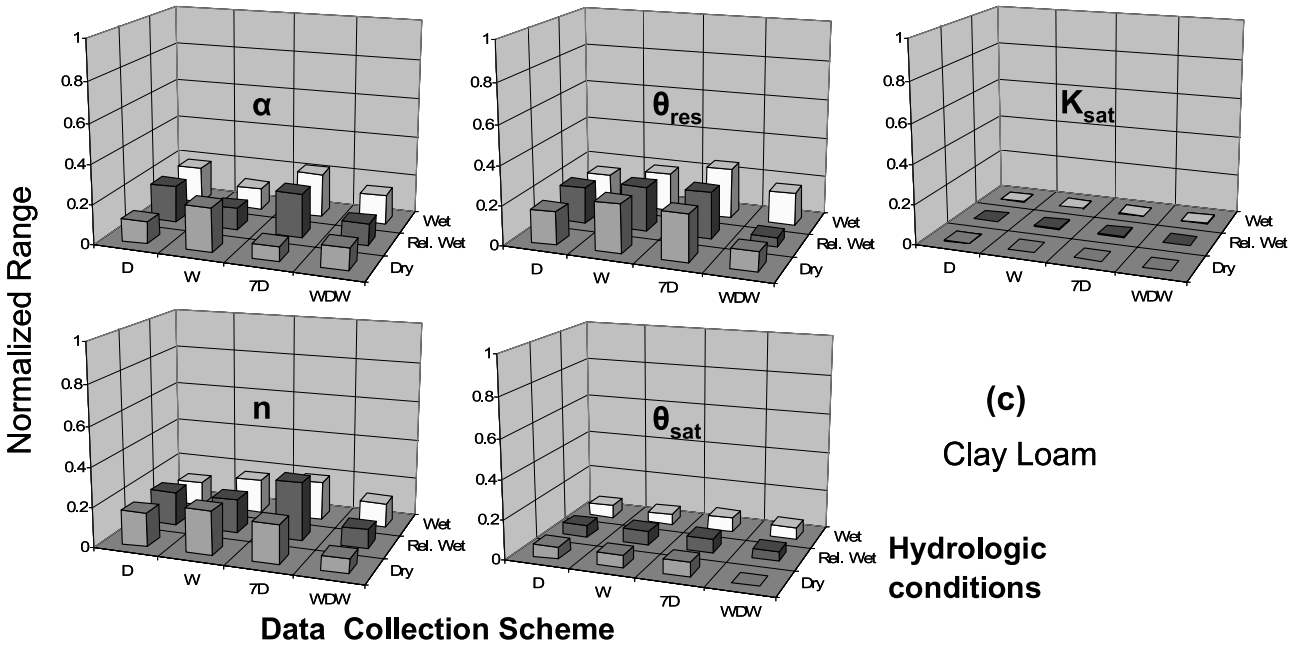

Figure 6c. Uniqueness of solutions for clay loam soils for case 1 under free-draining condition. D, daily; W, weekly; 7D, 7-day average; WDW, wet/dry window. Values are normalized based on the minimum and maximum values of the parameters from Table 1.

maximum rooting depth was 125 cm with a triangular root density, and the shallower rooting depth scenario was taken as 75 cm. All 10 realizations of the perturbed soil moisture data were used to estimate the effective soil hydraulic properties of the soil profile under all combinations of the rooting depth and root density scenarios.

2.3. Field Validation Experiment

[26] We applied our near-surface soil moisture assimilation scheme to a field validation site (ARS133) in the Little Washita watershed, Oklahoma, using in situ data from the Southern Great Plains 1997 (SGP97) hydrology experiment [see *Heathman et al.*, 2003; *Das and Mohanty*, 2006]. The ARS133 site has a sandy loam soil and grass ground cover. The SGP97 experiment was designed to study the variability of soil moisture within the remote sensing footprint and to analyze the physical controls of soil moisture dynamics at various spatial scales (from point, field, to remote sensing footprint) [*Mohanty and Skaggs*, 2001]. The near-surface and profile soil moisture data used in this study were measured using time domain reflectometry probes [*Heathman et al.*, 2003]. Daily weather data including solar radiation, precipitation, humidity, minimum and maximum temperature, and wind speed were collected from the USDA Agricultural Research Service Micronet weather station on-site and from nearby Oklahoma Mesonet stations. In this part of the study, simulations were done for 1 calendar year between 1 January and 31 December 1997 wherein the near-surface soil moisture (0–5 cm depth) collected during the SGP97 experiment (June–July 1997) were used as conditioning data for the parameter estimation. SWAP models grass as an annual crop with a growth cycle of 1 year. To account for uncertainties caused by initial and boundary conditions, we conducted the experiments using various combinations of boundary and initial conditions (imposed by water table depths of 200, 150, and 100 cm from the soil surface).

3. Results and Discussions

3.1. Numerical Case Studies

3.1.1. Case 1: Homogenous Free-Draining Column

[27] Figure 4 shows an example of a GA solution to the near-surface soil moisture assimilation procedure. The three lines in each panel indicate the performance of the three sets of initial populations used in the GA (see section 2.1.4). Notice the gradual improvements of the solutions as the generation progresses (Figure 4a). The stepwise improvement of the best chromosome is a unique characteristic of an elitist GA [*Ines and Droogers*, 2002]. The effect of the high creep mutation rate is also evident, and the effect of the intermittent jump mutation is noticeable as well (Figure 4b; see also Figure 5, the spikes in the case of K_{sat}). These perturbations on **k** are essential to better exploring the global search space, which has a maximum possible parameter combinations of 8,589,934,592 (see Table 1). Searching for the solution space by exhaustive enumeration would be impossible. With the multipopulation approach, a total of 15,000 parameter combinations (with replacements) were evaluated, translating to a much smaller (1.75×10^{-6}) fraction of the global search space being searched, thus being computationally more efficient than exhaustive enumeration. It is also noteworthy that all three populations have converged after the 500th generations (Figure 4c). The differences in the maximum fitness (Figure 4a) among the elite chromosomes of the three populations are attributed to the genetic makeups of the random number generator seeds; whether they are weak or strong, or how good are their genetic traits, which would indicate how long will it take for their offspring to evolve into better individuals. Figure 4a

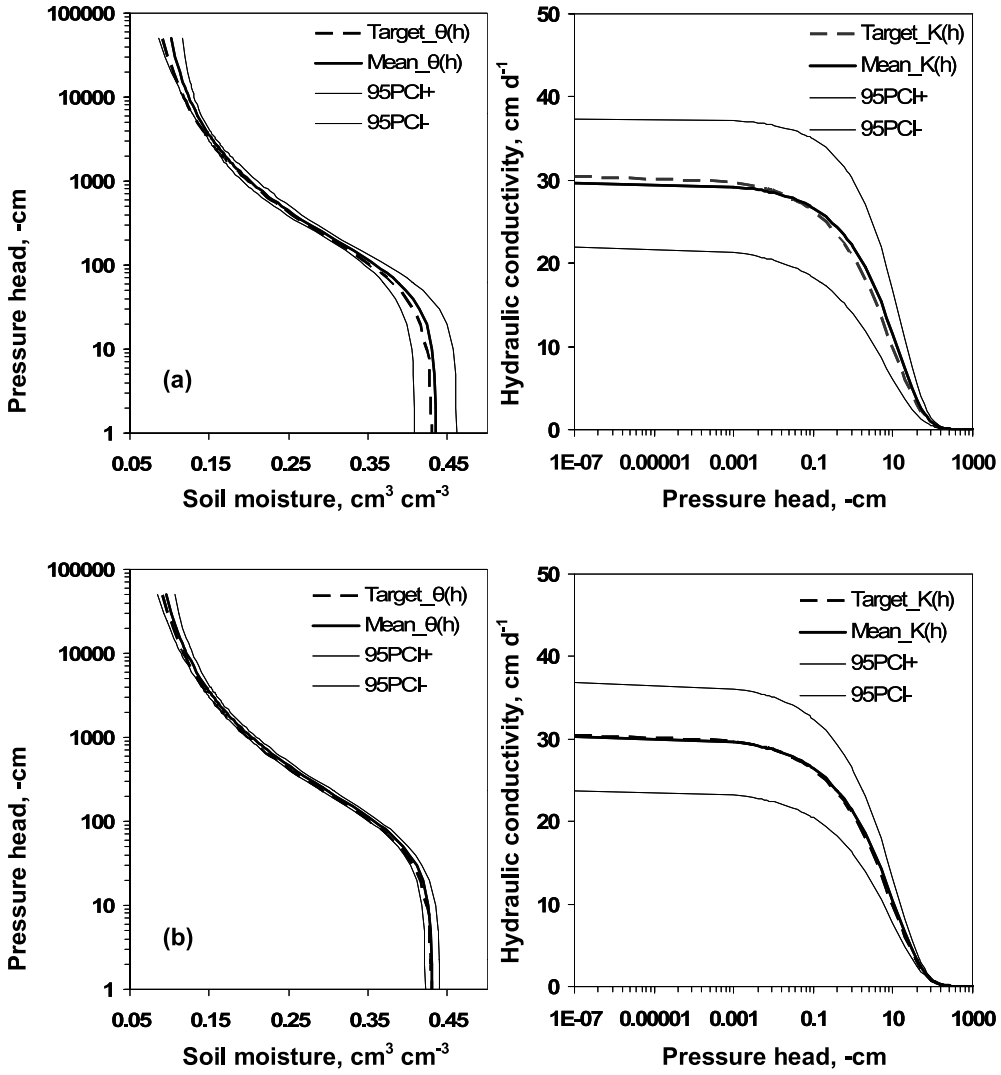

Figure 7. Derived θ(h) and K(h) for silt loam estimated using (a) daily interval and (b) wet/dry window scheme in case 1 during dry year.

indicates some degree of nonuniqueness among the fitness of the elite chromosomes at the end of the generations, but if these performances are translated into soil moisture errors (Figure 4c) the differences are rather minimal (Figure 4c). Figure 5 also shows a chronological GA search space exploration by one of the three populations used. It shows the power of the modified microGA to converge simultaneously albeit starting the search process from very weak positions at the search surface. After some time along the generations, all five soil hydraulic parameters converged closely within the vicinity of their expected values.

[28] Tables 2a–2c show the summary of results of the near-surface soil moisture assimilation for case 1 (Figure 2a) under different soil types and different hydroclimatic conditions. The estimated soil hydraulic parameters are shown in terms of their (arithmetic) means and 95PCI. In Table 2a, comparing the expected values and the estimated parameters (with modified microGA) showed that the sandy loam soil appeared to be easily identifiable during the dry year. On the average, the shape parameters α and n were properly identified (0.022 and 1.61, respectively) while the scale parameters (θ_{res}, θ_{sat}, and K_{sat}) showed small variations (in means) among the data collection/aggregation schemes used: 0.066–0.067 cm^3 cm^{-3} for θ_{res}, 0.372–0.375 cm^3 cm^{-3} for θ_{sat}, and 44.1–46.1 cm d^{-1} for K_{sat}. Their 95PCI showed that the derived soil hydraulic parameters honor their expected values wherein their bounds indicate the uncertainties of the GA solutions. Apparently, the uncertainties of α, n (except for the 7D scheme), and θ_{res} appeared to be smaller compared with θ_{sat} and especially K_{sat}. In general, these findings may suggest that the shape parameters (describing the nonlinearity) are better predictable with more accuracy than the scale parameters (describing the relative magnitude) for defining the water retention and hydraulic conductivity functions for sandy loam soil. The advantage of using the (physical) event-based WDW (wet/dry event window) data aggregation scheme for better matching the mean and constraining the spread of θ_{sat} and K_{sat} was not yet evident compared with using a daily (D) or weekly interval (W) data set. This result has practical implications in terms of hydrologic data collection protocols as the weekly interval scheme (W) faired well in performance during the dry year (Table 2a). Almost similar patterns were observed for the results in relatively wet

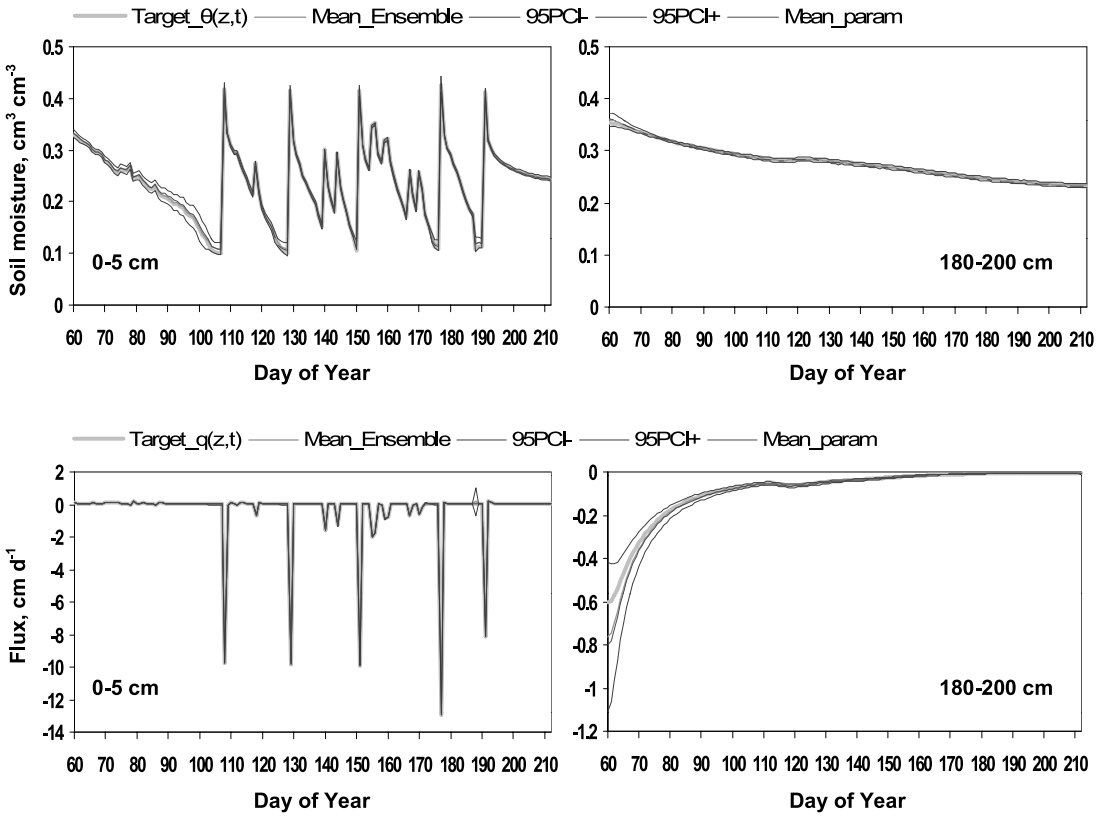

Figure 8a. (top) Daily soil moisture ($cm^3\ cm^{-3}$) and (bottom) flux ($cm\ d^{-1}$) at 0–5 cm and 180–200 cm depths of the silt loam column using θ(h) and K(h) derived from daily (D) interval data collection scheme during dry year (case 1, homogenous, free-draining soil column). Mean_Ensemble, mean of ensembles; mean_param, derived from the mean of parameter estimates.

and wet years in terms of the mean values of α, n, and θ_{res}, although mean values of θ_{sat} and K_{sat} appeared to be relatively larger than their expected values. This indicates the general insensitivities of θ_{sat} and K_{sat} to the parameter estimation during wetter conditions. Similar patterns (during the dry year) were also observed during the wetter years in terms of the uncertainty bands of all the soil hydraulic parameters. Overall, the method was found to be relatively robust in estimating the mean parameter values of α, n, θ_{res}, and θ_{sat} for the sandy loam soil (Table 2a). K_{sat} was relatively more variable (i.e., less unique) and that on the average had been of some orders of magnitude above the expected values for sandy loam (see Table 2a).

[29] Figure 6a further shows the uniqueness of the soil hydraulic parameter estimates for the sandy loam soil under all data collection/aggregation schemes used during the dry, relatively wet, and wet years considered. The plots in the Figure 6a were normalized based on the minimum and maximum parameter values given in Table 1. In general, there was a high degree of uniqueness for parameters n and θ_{res}, while moderate degrees of uniqueness for α and θ_{sat} and a fair degree of uniqueness for K_{sat} were observed. The mean values of n were properly defined (see Table 2a), and their uniqueness (range of 95PCI) was slightly variable among the different data collection/aggregation schemes and hydroclimatic conditions, suggesting that parameter n can be adequately defined across a range of hydroclimatic conditions and data collection protocols in sandy loam soils. In physical terms, this may again imply the significance of nonlinearity (reflected by n) in soil water retention and hydraulic conductivity functions for sandy loam soil.

[30] Table 2b shows the results of the silt loam soil. Generally, the results in the dry year were opposite the case of the sandy loam soil (Table 2a). The mean values of α were properly defined, and very good estimates were derived for θ_{sat} and K_{sat}. However, parameters n and θ_{res} were more variable than the results of the sandy loam soil. In this case, the WDW scheme performed better than the other data collection schemes (D, W, and 7D). It is interesting to note that there are data collection schemes whose 95PCI bounds did not capture well the expected values of several soil hydraulic parameters including 7D for α, and W for n and θ_{res} (in dry years), meaning they either greatly underestimated or overestimated their expected values. This result indicates that the hydraulic parameters of silt loam are more difficult to identify during the dry year. On the other hand, parameters α, n, θ_{res}, and θ_{sat} were better identified in the wet year. However, K_{sat} uncertainties were generally higher during the wet year (Table 2b). Figure 6b demonstrates that the uniqueness of α was variable. The parameter θ_{res} was more unique during the wetter years, while θ_{sat} was moderately unique for all the hydrologic years considered.

[31] To better understand the processes occurring in the soil profile during a dry or a wet year, we examined the correlations of soil moisture, pressure heads, and fluxes at different depths in the soil profile. Our analysis showed that during the dry year, the correlation of the near-surface soil moisture (0–5 cm) and the soil moisture in the subsurface

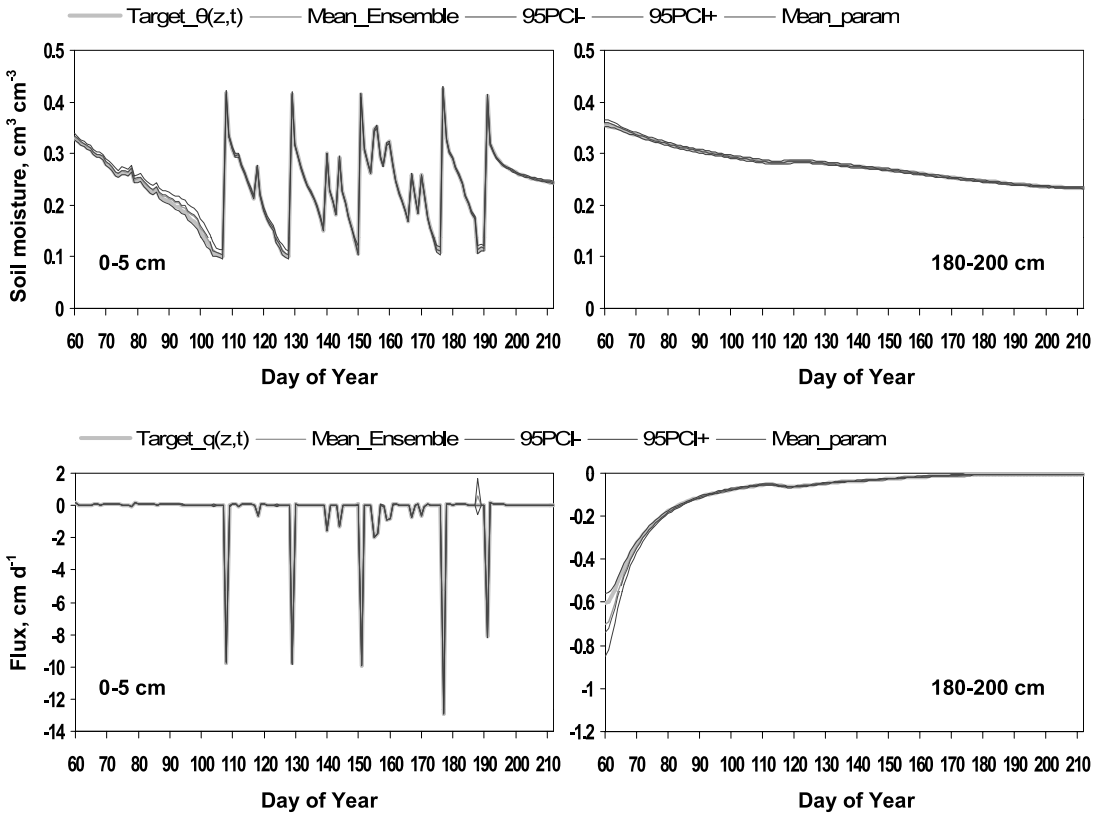

Figure 8b. (top) Daily soil moisture ($cm^3\ cm^{-3}$) and (bottom) flux ($cm\ d^{-1}$) at 0–5 cm and 180–200 cm depths of the silt loam column using θ(h) and K(h) derived from wet/dry window (WDW) scheme during dry year (case 1, homogenous, free-draining soil column). Mean_Ensemble, mean of ensembles; mean_param, derived from the mean of parameter estimates.

soil layers are lower compared with when it is a wet year. This suggests that the signature of the near-surface soil hydraulic processes within the subsurface soil layers are weaker during a dry year than in a wet year. The difference in the near-surface versus subsurface soil moisture correlations between dry and wet years is attributed to the difference in response times for the near-surface events to propagate in the subsurface soil layers. The degree of continuity/discontinuity in the pore spaces (based on saturation) is different in a wet and a dry year condition. We

Table 3. Solution of Genetic Algorithm to the Near-Surface Soil Moisture Assimilation for Case 2, Homogenous Column With Shallow Water Table (−150 cm) With WDW Scheme

		Dry Year		Relatively Wet Year		Wet Year	
Soil/Parameter	ExpectedValue[a]	Mean	95PCI	Mean	95PCI	Mean	95PCI
Sandy loam							
α	0.021	0.023	0.021–0.025	0.022	0.021–0.024	0.022	0.020–0.024
n	1.61	1.59	1.55–1.62	1.60	1.58–1.61	1.61	1.59–1.62
θ_{res}	0.067	0.066	0.065–.067	0.066	0.065–0.068	0.067	0.063–0.071
θ_{sat}	0.37	0.375	0.369–0.380	0.373	0.367–0.379	0.375	0.362–0.388
K_{sat}	41.6	50.2	39.8–60.6	46.5	37.0–55.9	46.7	30.8–62.7
Silt loam							
α	0.012	0.013	0.007–0.019	0.011	0.004–0.017	0.011	0.008–0.013
n	1.39	1.49	1.34–1.65	1.48	1.37–1.59	1.45	1.29–1.60
θ_{res}	0.061	0.116	0.035–0.197	0.091	0.060–0.123	0.071	0.050–0.092
θ_{sat}	0.43	0.433	0.378–0.487	0.429	0.353–0.506	0.428	0.371–0.485
K_{sat}	30.5	34.5	0.0–71.9	23.6	0.0–57.2	22.3	13.0–31.6
Clay loam							
α	0.030	0.029	0.027–0.032	0.030	0.028–0.031	0.030	0.027–0.033
n	1.37	1.35	1.32–1.38	1.38	1.35–1.41	1.40	1.37–1.42
θ_{res}	0.129	0.118	0.081–0.154	0.130	0.121–0.139	0.136	0.128–0.144
θ_{sat}	0.47	0.469	0.462–0.476	0.471	0.465–0.476	0.473	0.468–0.479
K_{sat}	1.84	1.92	1.75–2.09	1.88	1.83–1.93	1.89	1.80–1.97

[a]UNSODA database [*Leij et al.*, 1999].

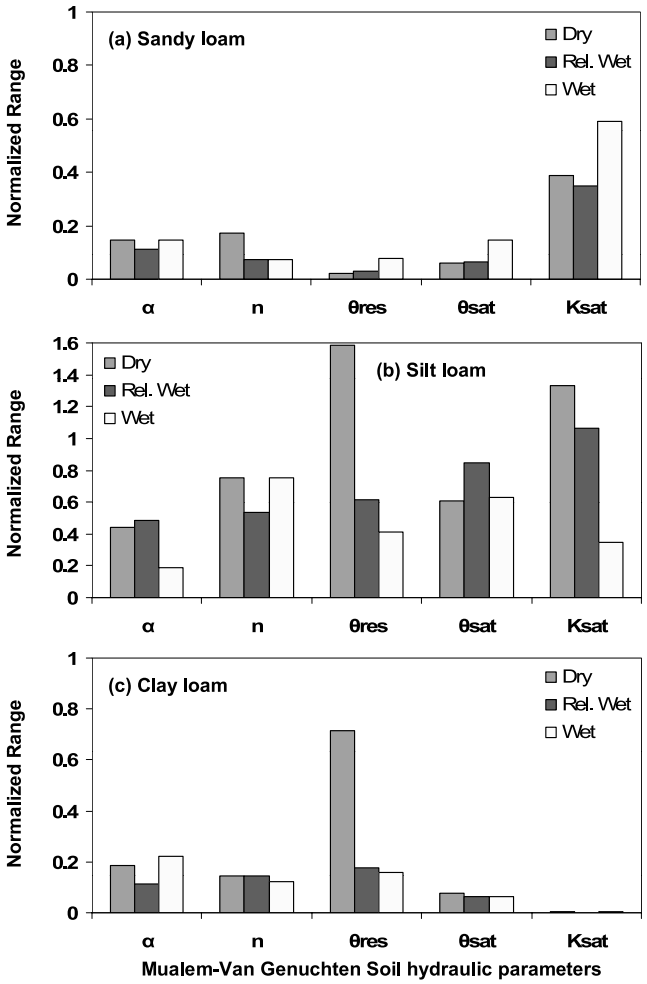

Figure 9. Uniqueness of solutions for (a) sandy loam, (b) silt loam, and (c) clay loam soils for case 2 with the presence of shallow water table (−150 cm) using wet/dry window (WDW) scheme.

hypothesize that during the dry year the dependence of θ_{res} and n is high in silt loam soils because of the discontinuity (i.e., air entrapment) in the soil matrix and as a result they are more difficult to identify.

[32] Table 2c shows the results for the clay loam soil. The hydraulic parameters of clay loam were better identified compared with sandy loam and silt loam soils. The mean soil hydraulic parameters (except θ_{res}) were properly estimated for both dry and wet years. The uncertainties of parameter estimates were also found to be small except for the parameter n. The 95PCI of the mean values were narrow and the mean parameter estimates were close to the expected values for all cases, which indicates that GA is highly effective in estimating the soil hydraulic parameters of clay loam for all (dry, relatively wet, wet) years considered. Figure 6c shows that the uniqueness of the parameter estimates ranged from high to moderate, demonstrating further the strong identifiability of clay loam soil by inverse modeling with GA.

3.1.1.1. Robustness of the Parameter Estimates

[33] Here we present only the case of the silt loam soil for the dry year condition using two (D and WDW) data collection/aggregation schemes. Figures 7a–7b show the θ(h) and K(h) curves using the parameter values from the GA solutions (Table 2b). For the (daily) D scheme, notice the effects of uncertainties of θ_{res}, n, and θ_{sat} on θ(h). The effects of the K_{sat} uncertainty can be also noticed in the K(h) curve. Comparing the estimated soil water retention θ(h) and hydraulic conductivity K(h) functions between the D and the (wet/dry window) WDW scheme, the improvements for the θ(h) derived from WDW scheme were considerable. On the other hand, the difference of the estimated K(h) between the two data collection schemes was less significant. These derived soil hydraulic parameters were then translated into soil hydrologic states by using them as inputs in the SWAP forward simulations. Figures 8a–8b show the simulated soil moisture contents and fluxes near the soil surface (0–5 cm) and the deeper (180–200 cm) layers of the soil profile. In Figure 8a (for the D scheme), the uncertainty of the simulated soil moisture during the drying event may be attributed to the uncertainty of θ(h) in the drier range of soil moisture (see Figure 7a). The uncertainty of fluxes near the bottom of the soil profile (180–200 cm depth) at the beginning of the simulation period (DOY 60–80) can be attributed to the uncertainty in the near-saturated range of θ(h) and K(h) (as shown in Figure 7). The uncertainty of soil water fluxes decreases for drier conditions because the derived K(h) matches well the expected values in the drier range (Figure 7a). Figure 8b shows the improvements of the simulated soil moisture contents and fluxes across the soil profile (i.e., for both shallow and deep layers) due to the improved estimates of the soil hydraulic parameters derived using the physically based WDW scheme. Evidently, the WDW scheme smoothened some of the uncertainties in the estimated θ(h) and K(h) functions. Note that these results are based on error-free conditions and that the effects of modeling and data uncertainties are not accounted for in the simulations of the subsurface processes. Hence, if the effective soil hydraulic parameters are properly estimated in the inverse modeling the subsurface processes are likely to be highly replicated. The effects of modeling (structural) and data errors on the simulated subsurface processes are discussed later, in section 3.1.4.

3.1.2. Case 2: Homogenous Column With Shallow Water Table

[34] Table 3 shows the summary of results of the near-surface soil moisture assimilation in the presence of a shallow water table at a depth of 150 cm from the soil surface (Figure 2b). In this case, we only used the WDW scheme in preparing the conditioning data for the parameter estimation. Table 3 shows that on the average the hydraulic parameters for the sandy loam and clay loam soils can still be identified with comparable results as with the ones derived under free-draining conditions (compare the Tables 2a and 2c WDW schemes). The parameter estimates, however, were more uncertain, especially for parameter n for both sandy loam and clay loam soils and θ_{res} for clay loam soil. For the silt loam soil, only the soil hydraulic parameters α and θ_{sat} were estimated more successfully. The performance of the silt loam soil in the presence of a shallow water table will be examined in-depth in the succeeding section. The uniqueness of the parameter estimates ranged from fair to high across the hydrologic dry through wet years with better uniqueness observed for

Table 4. Seasonal Water Balance (mm) With Shallow Water Table (−150 cm) for Cropping Season 1 Mar to 31 Jul (Dry Year)

	Sandy Loam				Silt Loam				Clay Loam			
Water Balance Components	Target Values[a]	Mean of Ensembles[b]	SD	Averaging Parameters[c]	Target Values	Mean of Ensembles	SD	Averaging Parameters	Target Values	Mean of Ensembles	SD	Averaging Parameters
Storage												
Final storage	595.90	597.98	3.18	597.40	774.80	776.23	27.09	775.40	876.80	853.27	23.45	838.00
Initial storage	598.30	600.35	3.22	599.80	776.20	777.58	27.33	776.60	795.90	796.52	10.04	797.40
Change	−2.40	−2.40	0.00	−2.40	−1.40	−1.32	0.22	−1.20	80.90	56.75	28.24	40.60
Incoming fluxes												
Rain	271.90	271.90	0.08	271.90	271.90	271.90	0.00	271.90	271.90	271.90	0.00	271.90
Irrigation	199.90	199.98	0.10	200.10	0.00	0.00	0.00	0.00	600.00	600.02	0.08	600.00
Bottom flux[d]	255.80	250.28	7.23	246.30	530.90	529.37	0.41	531.90	?78.40	?94.12	28.92	−112.80
Outgoing fluxes												
Interception	11.50	11.30	0.29	11.10	14.20	14.10	0.00	14.20	7.60	7.90	0.44	8.00
Runoff	0.00	0.00	0.00	0.00	0.00	0.00	0.00	0.00	85.20	79.45	7.15	79.10
Transpiration	614.10	608.90	7.47	605.00	685.70	683.89	0.54	686.50	472.10	477.52	8.94	478.80
Soil evaporation	104.40	104.35	0.90	104.50	104.40	104.58	0.10	104.30	147.60	151.78	11.11	152.00
Crack flow	0.00	0.00	0.00	0.00	0.00	0.00	0.00	0.00	0.00	0.00	0.00	0.00

[a]Simulated using the expected values of the parameter estimates.
[b]Average of water balance components from the ensemble of simulations.
[c]Water balance components derived from forward simulations using the arithmetic average of parameter estimates.
[d]Negative sign means the bottom flux is going out (downward in direction) from the control volume. Positive sign means the bottom flux is going into the control volume (upward in direction).

sandy loam and clay loam soils, while worst for the silt loam soil (Figures 9a–9c).

3.1.2.1. Robustness of the Parameter Estimates

[35] Table 4 shows the water balance generated from forward SWAP simulations with a shallow water table condition using the parameter estimates in Table 3 during a dry year (annual rainfall 330 mm). For sandy loam, although the seasonal bottom flux is positive, meaning upward in direction (going into the control volume), irrigation was still required because the capillary rise was not able to supply the seasonal crop water requirements. This particular response is attributed to the texture of the soil and the proximity of the water table from the rooting zone. The seasonal bottom flux covered only 35.6% of the seasonal ET (i.e., soil evaporation + transpiration). For the two wet years considered, the seasonal bottom fluxes covered 28.5% (cropping season rainfall, 199 mm; see Figure 3) and 31.6% (cropping season rainfall, 228 mm) of the seasonal ET, respectively (results not shown here). For the sandy loam, the soil hydrology was still dominated by downward flows caused by rainfall and irrigation and by redistribution in the soil profile. As shown in Table 4, the estimated soil hydraulic parameters were able to reproduce closely the water balance components within acceptable uncertainty bounds.

[36] In the case of the silt loam soil, most of the water needed by the wheat crop was supplied by the shallow water table through capillary rise combined with the moderate hydraulic conductivity of the soil. The bottom (upward) flux from the water table covered 67.2% of the seasonal ET during the dry year (Table 4) and covered 74.3% and 72.7% of seasonal ET during the wet years (not shown). The higher contributions of the groundwater to ET during the wet years were apparent because of the 84-mm rainfall event (see Figure 3) that occurred at the later stage of the growing season during the dry year, which supplied adequate water for crop use on that year. From these results we infer that the inability of the near-surface assimilation to characterize better the silt loam soil under a shallow water table could be attributed to the flow process conditions in the unsaturated zone. The flow process was predominantly controlled by the bottom boundary condition (upward fluxes) (see Table 4) and not by the near-surface processes, in which the conditioning data for the parameter estimation were derived.

[37] For the case of the clay loam soil, the capillary rise was not able to supply water in the root zone adequately, and thus irrigation was made by the SWAP model during the growing season. Although high capillarity was expected in fine-textured soils, the limited hydraulic conductivity (small K_{sat}) of the soil restricts the upward flow of water from the shallow water table to the rooting zone, limiting the transport of water for a limited period of time (i.e., a cropping season). Because of the higher uncertainty of the derived K_{sat} during the dry year (see Figure 9c), a wider spread of the simulated soil water storage was observed in the water balance (Table 4). However, during the wet years the parameter estimates were able to reproduce closely the water balance components with acceptable levels of uncertainty (not shown). Furthermore, the soil was predominantly draining as no major upward flows (i.e., mostly negative bottom fluxes) from the shallow water table were observed (Table 4).

3.1.2.2. Sensitivity to Water Table Depths

[38] We expanded our analysis to study the effects of shallow water table on the near-surface soil moisture assimilation by examining the sensitivities of the estimated soil hydraulic parameters by varying water table depths. Figure 10 shows the overall trends of the parameter estimates as a function of water table depths. The sandy loam soil shows a trend of improving identifiability of all of its soil hydraulic parameters as the water table depths become deeper. This result strengthens our observation that the parameter identifiability tends to be higher when the soil profile is dominated by downward flows. For the clay loam soil, however, there was no apparent trend in parameter sensitivity, as clay loam soil hydraulic parameters can be adequately identified for all hydrologic scenarios considered. For the case of the silt loam soil, it can be seen that there is no unique sensitivity trend among the parameter

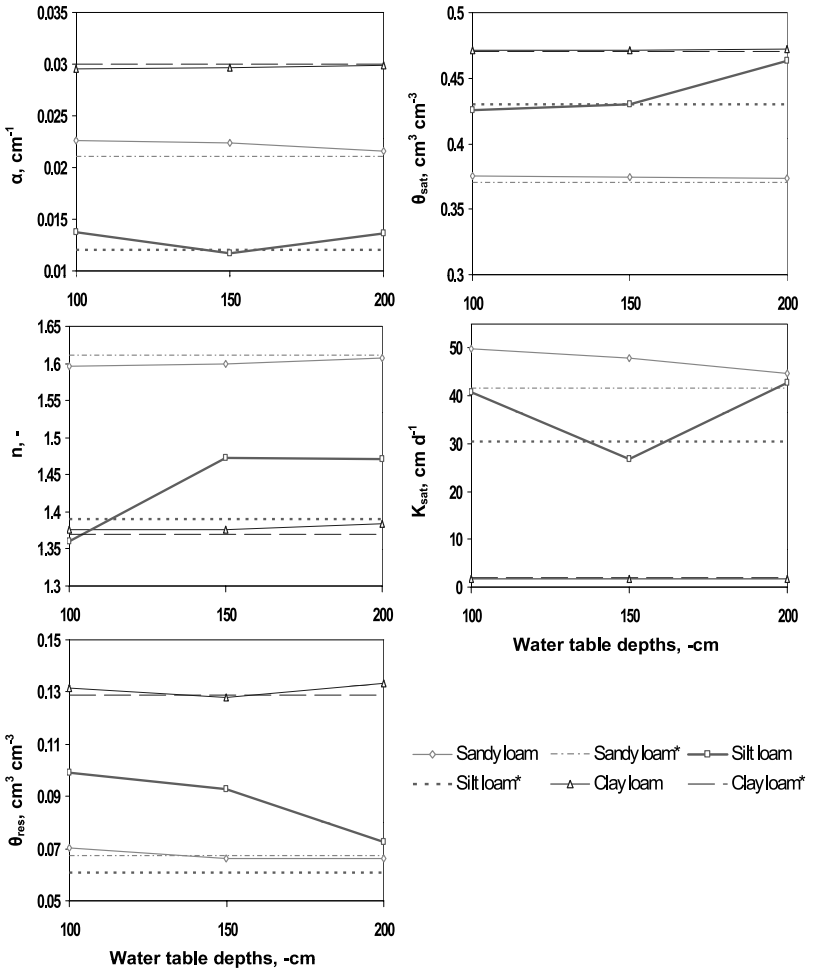

Figure 10. Parameter sensitivity to water table depths for sandy loam, silt loam, and clay loam, averaged for all years. Asterisk indicates target values.

estimates, as n and θ_{sat} tend to be more identifiable when the water table depth is shallower, while α and θ_{res} showed the opposite. On the contrary, K_{sat} did not show any clear trend at all. From these findings we suggest that the soil hydraulic parameters of the silt loam soil were not well identifiable because it was mostly dominated by upward flows from the shallow water table, and thus the processes in the unsaturated zone was primarily controlled by the bottom boundary condition and not by the near-surface processes that were used in the parameter estimation. Even at 200 cm water table depth, the bottom flux covered about 44.2–51.2% of the seasonal ET (not shown). We observed, however, that when the contributions of the bottom flux are lesser (during the wet year when most of the flow processes are vertically downward), the soil hydraulic parameters were fairly estimated.

3.1.3. Case 3: Heterogeneous Profile

[39] Figures 11a–11d show the results of the experiments during the dry year for a heterogeneous profile (Figure 2c) using the following search criteria: (1) near-surface soil moisture data (SM) only, (2) combined 0.6 SM and 0.4 ET, (3) combined 0.5 SM and 0.5 ET, and (4) combined 0.4 SM and 0.6 ET. These fractional values were selected to reflect the relative contributions of ET and soil moisture to the objective function (see equation (3a)). ET was considered to be a surrogate variable that could influence the processes occurring in the deeper layers of the soil profile and could potentially improve the identifiability of the subsurface soil hydraulic properties in the parameter estimation. It is evident that increasing the number of unknown parameters (with increasing number of soil layering) for the inverse modeling has resulted in higher parameter uncertainties. Nevertheless, the procedure was able still to provide fairly good results for several of the cases studied. Figure 11a demonstrates that using near-surface soil moisture data alone was capable of identifying hydraulic parameters of the topsoil layer (sandy loam) but not sufficient for identifying parameters of the bottom layer (silt loam) (see Figure 2c). In the second layer, the mean values of parameters α and θ_{sat} were well defined but with large uncertainties (numerical values not shown here), θ_{res} was overestimated, and K_{sat} was characterized also by high uncertainties. Figure 11b shows the effect of adding 0.4 ET to the conditioning criteria (0.6SM). Apparently using both soil moisture (f = 0.6) and ET (1 – f = 0.4) in the optimization problem has resulted in improved parameter estimates for the second/deeper layer, particularly for K_{sat}. With the additional conditioning data, the uncertainty bounds of θ(h) have also decreased, but the estimates of θ_{sat} and θ_{res} were still slightly off from their expected values. In the first soil layer, the mean values of θ_{sat} and θ_{res}

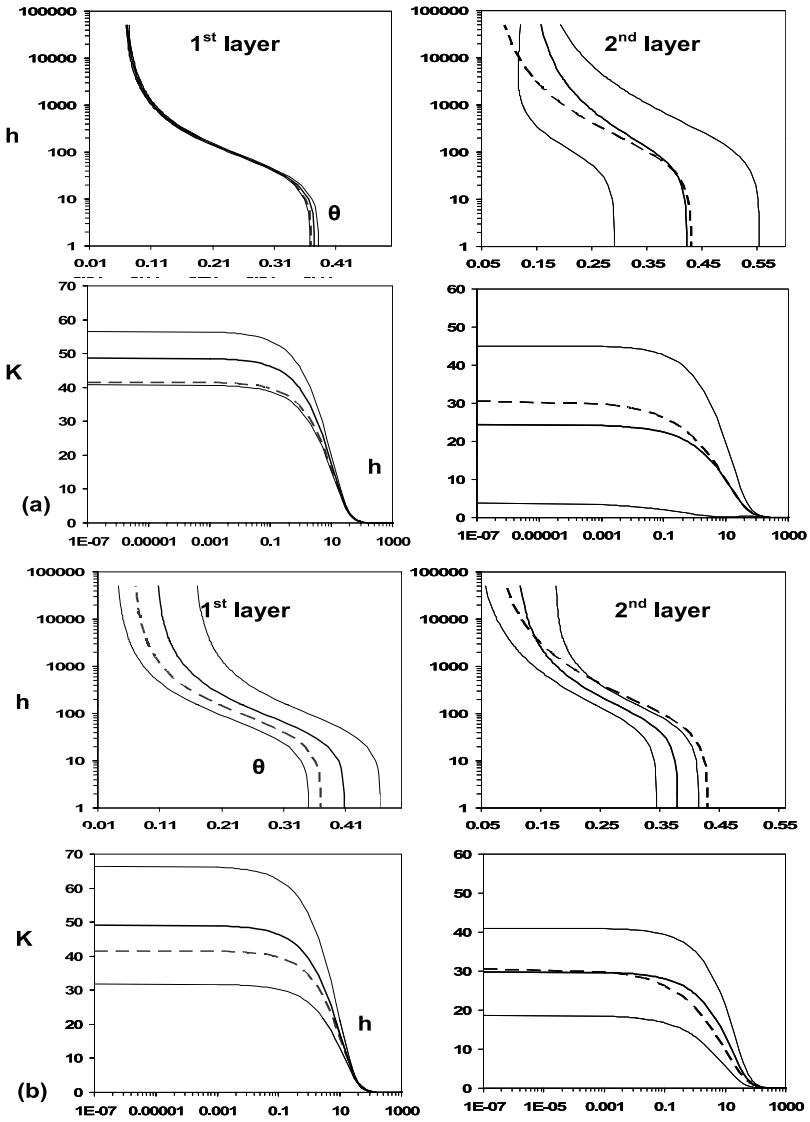

Figure 11. Solutions of the layered soil using (a) near-surface soil moisture (SM) only, (b) 0.6 SM and 0.4 ET, (c) 0.5 SM and 0.5 ET, and (d) 0.4 SM and 6 ET, as matching criteria during the dry year. Dashed line, target values; thick line, mean GA solutions; thin lines, 95 PCI; θ (cm^3 cm^{-3}), K (cm d^{-1}), h (per cm).

did not match well to their expected values, and uncertainties of K_{sat} estimates have increased noticeably (compare Figure 11b and Figure 11a). Now, only the shape parameters α and n were better defined after the additional conditioning. Nevertheless, the estimated θ(h) and K(h) functions for both first and second soil layers were better (Figure 11b) than when using only the near-surface soil moisture as conditioning data (Figure 11a). Figure 11c also shows the effects of adding 0.5 ET to the conditioning criteria (equation (3a)). The parameter estimates improved slightly for both first and second soil layers. Adding more weights to ET in the conditioning criteria did not show any further improvements to the parameter estimates (see Figure 11d). During wet years (not shown), almost similar trends were observed, while K_{sat} estimates for the second soil layer were always overestimated. The improvements made in the parameter estimates when ET was used as additional conditioning data suggest that the evapotranspiration front, which is the zone where root activities are active within the soil profile, is capable of (indirectly) providing information about the hydraulic properties of the subsurface soil layers.

3.1.4. Parameter Estimation Under Uncertainty

[40] Figure 12a shows the effects of data errors on the parameter estimation, i.e., using imperfect near-surface soil moisture data with perfect modeling assumptions (see section 2.2.2.4) in our numerical studies. Apparently, even with an assumed 20% error in the data sets (for all 10 realizations), the estimation of θ(h) was not greatly impaired. This result suggests that as long as the modeling domain is properly defined, the potential of estimating θ(h) using data with moderate errors in the parameter estimation is relatively high. K(h), however, was overestimated at the wetter range and with high uncertainty. Figure 13a shows

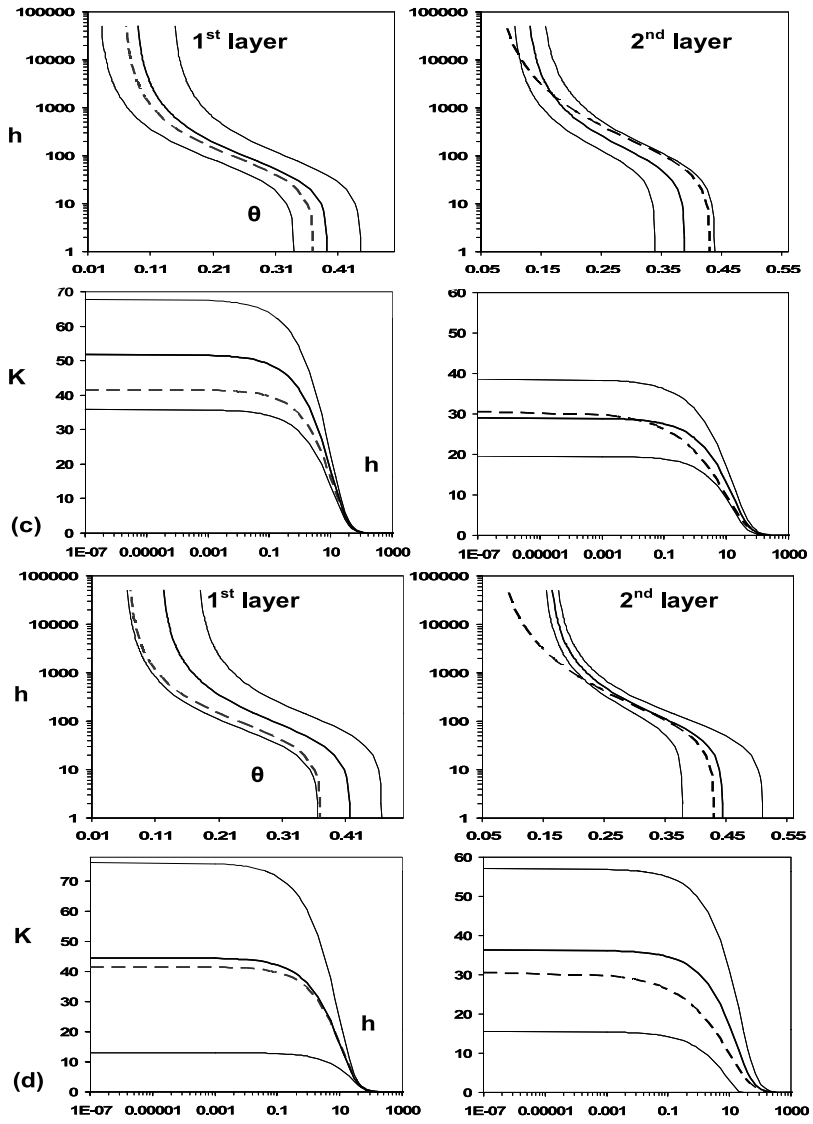

Figure 11. (continued)

the performance of the derived soil hydraulic functions in simulating the near-surface (0–5 cm) and subsurface (50–60 cm) soil moisture contents. The simulated mean soil moisture contents (both surface and subsurface) corresponded well with the target values and the uncertainties of the soil hydraulic parameter estimates (Figure 12a) were manifested more in the deeper soil layer (50–60 cm) than the near-surface soil layer.

[41] Figures 12b and 12c also show the effects of modeling errors on the parameter estimation in this numerical study. For Figures 12b and 12c we used perfect near-surface soil moisture data under imperfect modeling assumptions in the inverse modeling, i.e., varied rooting depth (Figure 12b) and varied root density (Figure 12c), respectively. Remarkably, even with varied (shallow) rooting depth (and base case scenario root density) and varied root density (and base case scenario rooting depth), the mean soil water retention curve θ(h) was estimated fairly well while K(h) was still overestimated at the wetter range at varying uncertainty levels. K(h) was more uncertain in the case of improper assumption of root density than for rooting depth (Figures 12b and 12c). However, it is also clear that the subsurface soil moisture (50–60 cm) was overestimated (wetter) with shallower rooting depth/triangular root density, and underestimated (dryer) with deeper rooting depth/trapezoidal root density (see section 2.2.2.4) during the drying phases in the simulations (Figures 13b and 13c). The uncertainty in the simulated subsurface soil moisture was higher if the root density is not properly defined. Evidently, the simulated near-surface soil moisture was dryer under the shallower root condition (base case scenario root density) due to more active upper rooting zone and wetter under the trapezoidal root density (base case scenario rooting depth) due to more active lower rooting zone (see Figures 13b and 13c).

[42] In the real world, however, data and modeling errors we encounter are more of a norm than deviations. Figures 12d and 13d show the combined effects of data and modeling

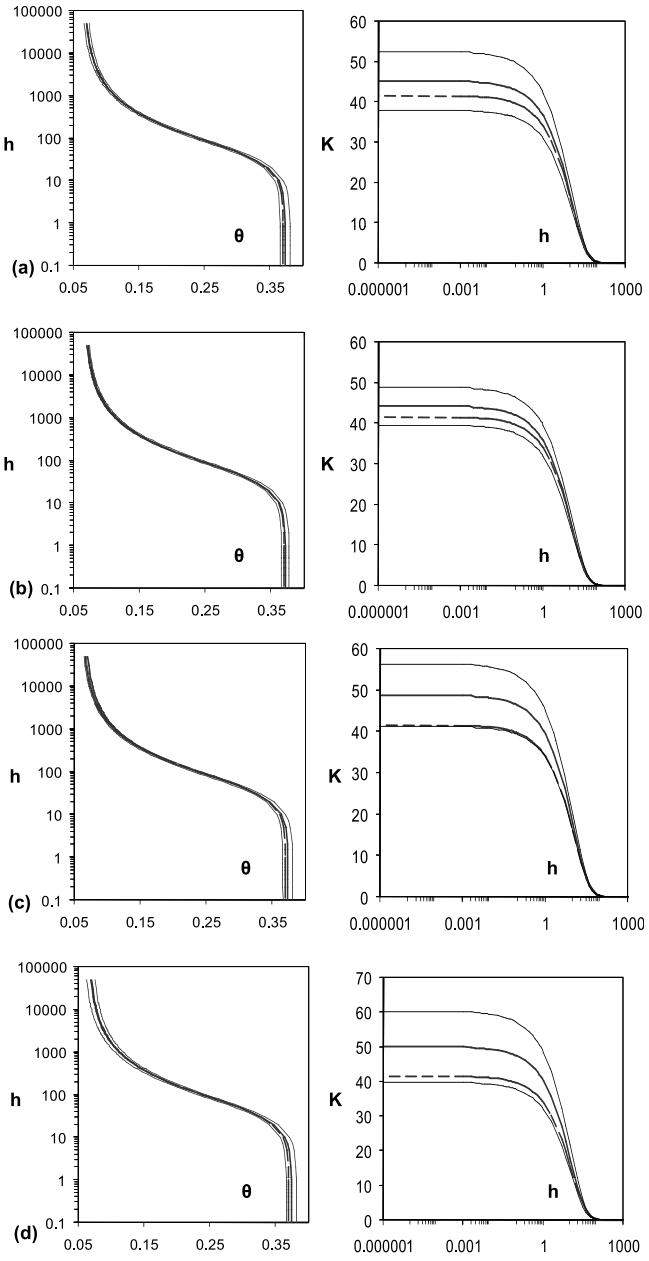

Figure 12. Derived soil hydraulic functions θ(h) and K(h) under (a) imperfect data (10 realizations)/perfect modeling condition (base case scenario rooting depth/base case scenario root density); (b) perfect data (base scenario)/ imperfect modeling condition (varied rooting depth/base case scenario root density); (c) perfect data (base scenario)/ imperfect modeling condition (base case scenario rooting depth/varied root density); and (d) imperfect data/imperfect modeling condition (varied rooting depth/varied root density). Dashed line, target values; thick line, mean GA solutions; thin line, 95 PCI; θ (cm^3 cm^{-3}), K (cm d^{-1}), h (per cm).

errors to the performance of the parameter estimation. Here we solved the inverse problem using imperfect modeling assumptions (rooting depth and root density) with data errors (all 10 realizations; see section 2.2.2.4). The combined effects of errors in data and modeling assumptions can be seen in the uncertainties of the estimated θ(h) and K(h) (Figure 12d), and in the simulated near-surface (0–5 cm) and subsurface (50–60 cm) soil moisture (Figure 13d) consistent with the findings of *Yang et al.* [2005]. Because of the increased number of ensemble members, the correspondence between the mean simulated and target soil moisture contents (both surface and subsurface) have improved. Apparently, K(h) was overestimated and more uncertain while θ(h) was estimated fairly well with lesser uncertainty, which suggests that the estimation of θ(h) by inverse modeling is less sensitive to the effects of data and modeling errors. This could be true assuming that the information content of the data (range, variability, type) is adequate to define the driest to wettest regions of the soil water retention curve.

3.2. Field Validation Experiment

[43] Figure 14 shows the derived θ(h) and K(h) at the (field) validation site ARS133 with a sandy loam soil and grass cover at the Little Washita watershed, Oklahoma [*Heathman et al.*, 2003]. Figure 15 also shows the daily rainfall during the SGP97 hydrology campaign and the simulated near-surface (0–5 cm) and subsurface (0–60 cm) soil moisture contents using the derived θ(h) and K(h) (shown in Figure 14) as inputs in the forward SWAP simulations. The estimated effective θ(h) matched well the measured θ(h) derived from laboratory measurements (Figure 14a) using a soil core extracted near the ARS 133 site [*Mohanty et al.*, 2002]. The estimated θ(h) also corresponded well with the UNSODA data for sandy loam [*Leij et al.*, 1999] and showed even better results at the drier end of the water retention curve derived from laboratory measurements, which highlights the value of using actual field data in determining the hydraulic properties of field soils. These results further confirm the high identifiability of sandy loam soil by inverse modeling with a genetic algorithm. Since we did not consider macropore effects in our inverse analyses, the estimated K(h), particularly K_{sat}, did not match well with the average K_{sat} (sandy loam) in the Little Washita watershed and SGP97 region. Nevertheless, the estimated θ(h) and K(h) reproduced well the near-surface (0–5 cm) (R = 0.94; MBE = 0.006 cm^3 cm^{-3}) and subsurface (0–60 cm) (R = 0.83; MBE = −0.025 cm^3 cm^{-3}) soil moisture dynamics when used in the forward modeling with SWAP.

4. Concluding Remarks

[44] This paper presents a near-surface soil moisture assimilation procedure that can be used to quantify effective soil hydraulic parameters in the soil profile. The approach included an indirect way of assimilating the near-surface soil moisture data into soil hydrologic models to derive saturated and unsaturated hydraulic conductivity K(h) and soil water retention θ(h) properties of the soil. We used a modified microGA to search for the solutions of θ(h) and K(h) via inverse modeling using a one-dimensional soil hydrologic model, SWAP. The approach also allows us to evaluate the uncertainties of the solutions, although the GA uncertainty assessment presented here may be considered ad hoc as it is not of the Bayesian type. We studied three

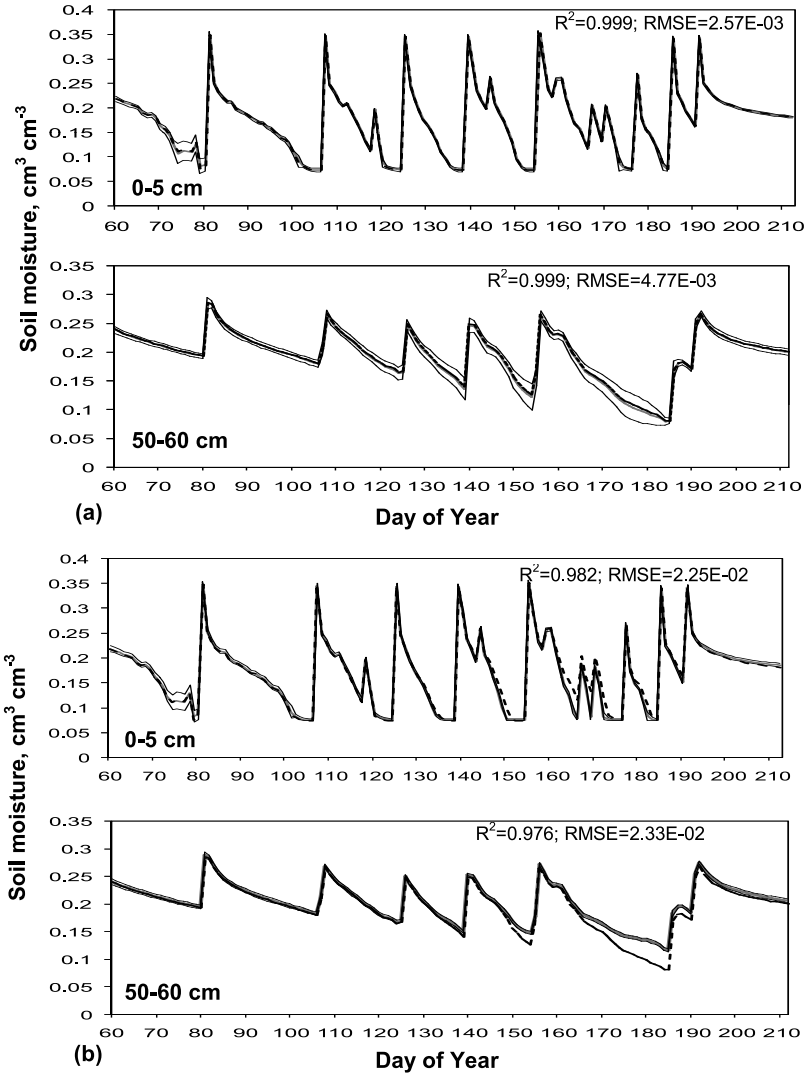

Figure 13. Simulated versus target soil moisture at 0–5 cm and 50–60 cm depths under (a) imperfect data (10 realizations)/perfect modeling condition (base case scenario rooting depth/varied root density); (b) perfect data (base scenario)/imperfect modeling conditions (varied rooting depth/varied root density); (c) perfect data (base scenario)/imperfect modeling condition (base case scenario rooting depth/varied root density); and (d) imperfect data (10 realizations)/imperfect modeling conditions (varied rooting depth/varied root density). Thick dashed line, target values; thin lines, 95 PCI; thick faded line, simulated soil moisture.

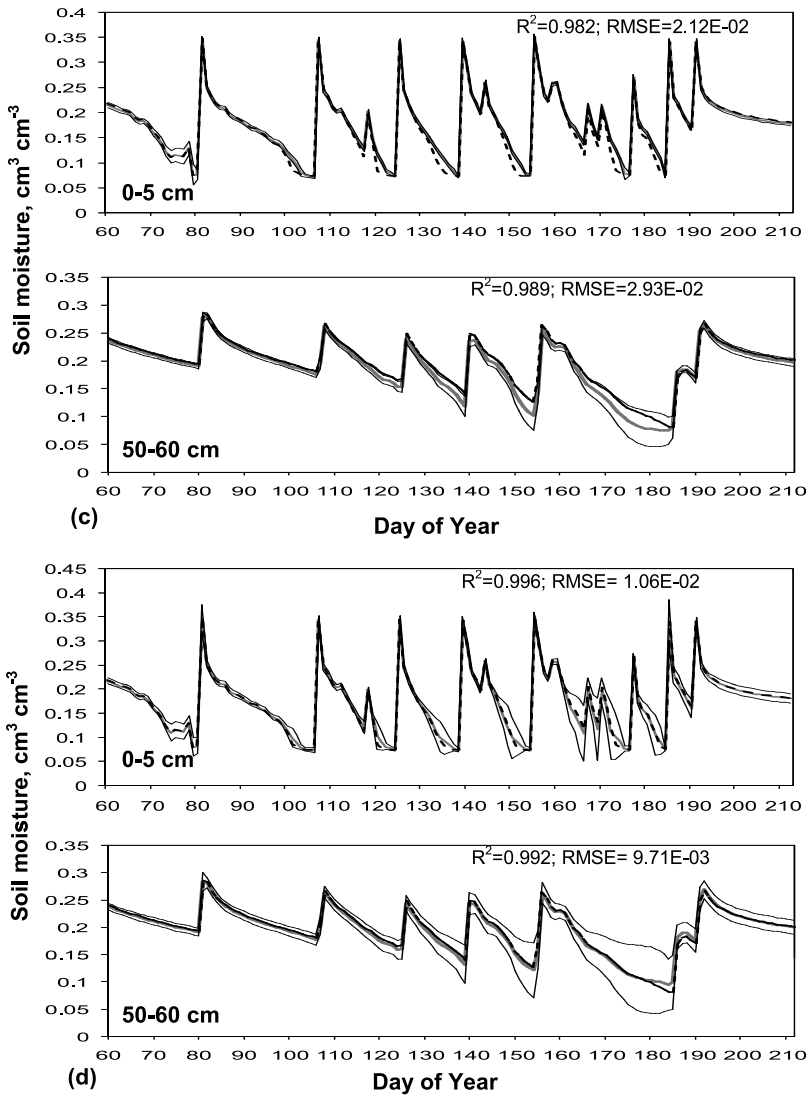

Figure 13. (continued)

different cases including a homogenous free-draining soil column (case 1), a homogenous soil column in the presence of a shallow water table (case 2), and a heterogeneous soil column (case 3). For cases 1 and 2 we considered three different soil textures, sandy loam, silt loam, and clay loam, as our tests for porous media, and for case 3 we used a two layered system of silt loam overlain by sandy loam. Generally, our results showed that the identifiability of soil hydraulic parameters increased as we approached the outer ranges of the soil textural class (clay loam – sandy loam). Most of the soil hydraulic parameters can be adequately identified for coarse- and fine-textured soils. We observed some difficulties in the identification of the moderate textured soil (silt loam) especially when the soil is dry. We found that flow regimes significantly controlled by the bottom boundary condition (i.e., upward flux from shallow water table) were less successful for the parameter estimation using near-surface soil moisture information. This result suggests that soil hydraulic parameters are better identified when the soil profile is predominantly draining than when the soil is predominantly wetting by upward flows from a shallow water table. However, when the contributions of the (upward) bottom flux from the shallow water table to the seasonal ET are less than 50%, the soil hydraulic parameters can be sufficiently identified using mainly near-surface soil moisture information in the parameter estimation. For the case of layered soil systems, the approach was not quite successful and only certain parameters could be identified. With soil moisture alone as conditioning criterion, we were able to define the soil hydraulic properties adequately for the first soil layer. This result was expected due to the direct relationship of the soil water retention and hydraulic properties of the first layer to the near-surface soil moisture data. Adding ET as conditioning criterion has improved the identification of the hydraulic parameters for the second layer, although not all parameters are highly identifiable. Using weights between 0.4 and 0.5 to ET (i.e., 0.6–0.5 SM) into the conditioning criteria has resulted in improved

estimates of the soil hydraulic parameters in the second layer. Overall, the shape parameters α and n of the Mualem-Van Genuchten functions defining the nonlinearity are the most highly identifiable parameters in both the top and bottom layers of the layered soil system case studies. We also conducted parameter estimations under uncertainties (data and modeling errors) and found that θ(h) could still be reasonably estimated while K(h) was more uncertain. The combined effects of data and modeling errors affect the uncertainties of the simulated soil moisture in the subsurface. Finally, the high identifiability of the effective soil hydraulic properties of sandy loam soils (especially for θ(h)) was demonstrated by applying the near-surface soil moisture assimilation scheme using in situ data from a field validation site in Little Washita watershed, Oklahoma.

[45] **Acknowledgments.** The research was funded by NASA-GAPP grant NNG04GM35G. We would like to acknowledge the partial supports of LANL-SAHRA, NASA (JPL and THP) and NSF (CMG/DMS and MRI), and NIH (EHS) grants for this work. We thank also the editors and reviewers for helping us improve the quality of the paper.

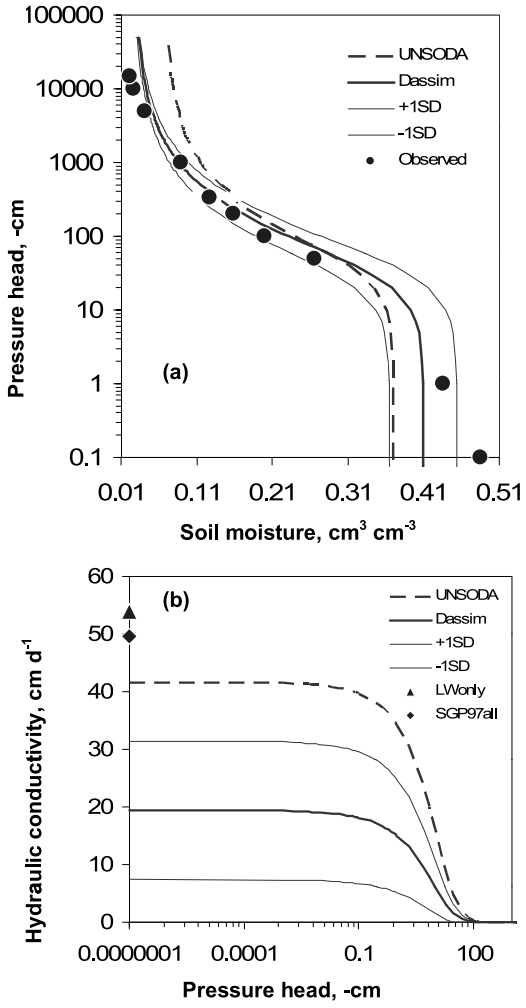

Figure 14. Derived effective (a) θ(h) and (b) K(h) of field validation site ARS133 (sandy loam) of Little Washita watershed, Oklahoma [see *Ines and Mohanty*, 2008]. LWonly designates mean of all measured K_{sat} (sandy loam sites) at Little Washita; SGP97 all designates mean of all measured K_{sat} (sandy loam sites) in SGP97 region.

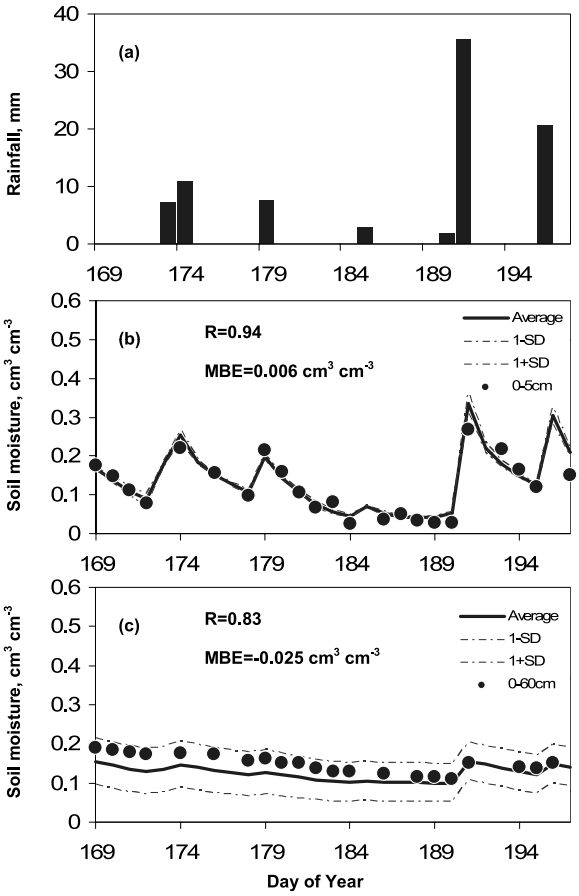

Figure 15. (a) Rainfall data, (b) observed and simulated near-surface (0–5 cm) soil moisture, and (c) observed and simulated subsurface (0–60 cm) soil moisture of the field validation site ARS133 (sandy loam) of Little Washita watershed, Oklahoma [see *Ines and Mohanty*, 2008]. Simulated soil moistures were produced using the derived effective soil hydraulic properties.

References

Abbaspour, K. C., M. T. Van Genuchten, R. Schulin, and E. Schläppi (1997), A sequential uncertainty domain inverse procedure for estimating subsurface flow and transport parameters, *Water Resour. Res.*, *33*, 1879–1892, doi:10.1029/97WR01230.

Abbaspour, K. C., R. Schulin, and M. T. van Genuchten (2001), Estimating soil hydraulic parameters using ant colony optimization, *Adv. Water Resour.*, *24*, 827–841, doi:10.1016/S0309-1708 (01)00018-5.

Antonopoulos, V. Z. (2000), Modeling of soil water dynamics in an irrigated corn field using direct and pedo-transfer functions for hydraulic properties, *Irrig. Drain. Syst.*, *14*, 325–342, doi:10.1023/A:1006453204285.

Belmans, C., J. G. Wesseling, and R. A. Feddes (1983), Simulation of water balance of a cropped soil: SWATRE, *J. Hydrol.*, *63*, 271–286.

Burke, E. L., R. J. Gurney, L. P. Simmonds, and T. J. Jackson (1997), Calibrating a soil water and energy budget model with remotely sensed data to obtain quantitative information about the soil, *Water Resour. Res.*, *33*, 1689–1697, doi:10.1029/97WR01000.

Burke, E. L., R. J. Gurney, L. P. Simmonds, and P. E. O'Neill (1998), Using a modeling approach to predict soil hydraulic properties from passive microwave measurements, *IEEE Trans. Geosci. Remote Sens.*, *36*, 454–462, doi:10.1109/36.662729.

Campbell, G. S. (1974), A simple method for determining unsaturated conductivity from moisture retention data, *Soil Sci.*, *117*, 311–314, doi:10.1097/00010694-197406000-00001.

Chang, D.-H., and S. Islam (2000), Estimation of soil physical properties using remote sensing and artificial neural networks, *Remote Sens. Environ.*, *74*, 534–544, doi:10.1016/S0034-4257 (00)00144-9.

Chan-Hilton, A. B., and T. B. Culver (2000), Constraint handling for genetic algorithms in optimal remediation design, *J. Water Resour. Plann. Manage.*, *125*, 128–137, doi:10.1061/(ASCE)0733-9496(2000)126:3(128).

Cieniawski, S. E., J. W. Eheart, and S. Ranjithan (1995), Using genetic algorithms to solve a multiobjective groundwater monitoring problem, *Water Resour. Res.*, *31*, 399–409, doi:10.1029/94WR02039.

Crow, W. T., and E. F. Wood (2003), The assimilation of remotely sensed soil brightness temperature imagery into a land surface model using ensemble Kalman filtering: A case study based on ESTAR measurements during SGP97, *Adv. Water Resour.*, *26*, 137–149, doi:10.1016/S0309-1708(02)00088-X.

Das, N. N., and B. P. Mohanty (2006), Root zone soil moisture assessment using remote sensing and vadose zone modeling, *Vadose Zone J.*, *5*, 296–307, doi:10.2136/vzj2005.0033.

Demarty, J., C. Ottlé, I. Barud, A. Olioso, J. P. Frangi, H. V. Gupta, and L. A. Bastidas (2005), Constraining a physically based Soil-Vegetation-Atmosphere Transfer model with surface water content and thermal infrared brightness temperature measurements using a multiobjective approach, *Water Resour. Res.*, *41*, W01011, doi:10.1029/2004WR003695.

Droogers, P., W. G. M. Bastiaanssen, M. Beyazgül, Y. Kayam, G. W. Kite, and H. Murray-Rust (2000), Distributed agro-hydrological modeling of an irrigation system in western Turkey, *Agric. Water Manage.*, *43*, 183–202, doi:10.1016/S0378-3774 (99)00055-4.

Dunne, S., and D. Entekhabi (2005), An ensemble-based reanalysis approach to land data assimilation, *Water Resour. Res.*, *41*, W02013, doi:10.1029/2004WR003449.

Entekhabi, D., H. Nakamura, and E. G. Njoku (1994), Solving the inverse problem for soil moisture and temperature profiles by sequential assimilation of multifrequency remotely sensed observations, *IEEE Trans. Geosci. Remote Sens.*, *32*, 438–448, doi:10.1109/36.295058.

Entekhabi, D., et al. (2004), The hydrosphere state (Hydros) satellite mission: An Earth system pathfinder for global mapping of soil moisture and land freeze/thaw, *IEEE Trans. Geosci. Remote Sens.*, *42*, 2184–2195, doi:10.1109/TGRS.2004.834631.

Feddes, R. A., P. J. Kowalik, and H. Zarandy (1978), *Simulation of Field Water Use and Crop Yield*, *simul. monogr.*, Pudoc, Wageningen, Netherlands.

Feddes, R. A., G. H. De Rooij, J. C. Van Dam, P. Kabat, and P. Droogers (1993a), Estimation of regional effective soil hydraulic parameters by inverse modeling, in *Water Flow and Solute Transport in Soils*, edited by D. Russo and G. Dagan, pp. 211–233, *Adv. Ser.* in Agric. Sci., Berlin.

Feddes, R. A., M. Menenti, P. Kabat, and W. G. M. Bastiaanssen (1993b), Is large-scale inverse modeling of unsaturated flow with areal average evaporation and surface soil moisture as estimated by remote sensing feasible? J, *Hydrol.*, *143*, 125–152, doi:10.1016/0022-1694(93)90092-N.

Galantowicz, J. F., D. Entekhabi, and E. G. Njoku (1999), Tests of sequential data assimilation for retrieving profile soil moisture and temperature from observed L-band radiobrightness, *IEEE Trans. Geosci. Remote Sens.*, *37*, 1860–1870, doi:10.1109/36.774699.

Goldberg, D. E. (1989), *Genetic Algorithms in Search and Optimization and Machine Learning*, Addison-Wesley, Boston, Mass.

Gwo, J.-P. (2001), In search of preferential flow paths in structured porous media using simple genetic algorithm, *Water Resour. Res.*, *37*, 1589–1601, doi:10.1029/2000WR900384.

Heathman, G. C., P. J. Starks, L. R. Ahuja, and T. J. Jackson (2003), Assimilation of surface soil moisture to estimate soil water content, *J. Hydrol.*, *279*, 1–17, doi:10.1016/S0022-1694(03)00088-X.

Holland, J. H. (1975), *Adaptation in Natural and Artificial Systems*, Univ. of Mich. Press, Ann Arbor.

Ines, A. V. M., and P. Droogers (2002), Inverse modeling in estimating soil hydraulic functions: A genetic algorithm approach, *Hydrol. Earth Syst. Sci.*, *6*, 49–65.

Ines, A. V. M., and K. Honda (2005), On quantifying agricultural and water management practices from low spatial resolution RS data using genetic algorithms: A numerical study for mixed pixel environment, *Adv. Water Resour.*, *28*, 856–870, doi:10.1016/j.advwatres.2004.11.015.

Ines, A. V. M., and B. P. Mohanty (2008), Near-surface soil moisture assimilation to quantify effective soil hydraulic properties under different hydro-climatic conditions, *Vadose Zone J.*, *7*, 39–52, doi:10.2136/vzj2007.0048.

Jackson, T. J., D. M. Le Vine, T. J. Schmugge, and F. R. Schiebe (1995), Large area mapping of soil moisture using ESTAR passive microwave radiometer in Washita '92, *Remote Sens. Environ.*, *54*, 27–37, doi:10.1016/0034-4257(95)00084-E.

Jhorar, R. K., W. G. M. Bastiaanssen, R. A. Feddes, and J. C. Van Dam (2002), Inversely estimating soil hydraulic functions using evapotranspiration fluxes, *J. Hydrol.*, *258*, 198–213, doi:10.1016/S0022-1694 (01)00564-9.

Kabat, P., R. W. A. Hutjes, and R. A. Feddes (1997), The scaling characteristics of soil parameters: From plot scale heterogeneity to subgrid parameterization, *J. Hydrol.*, *190*, 363–396, doi:10.1016/S0022-1694(96)03134-4.

Kerr, Y., P. Waldteufel, J.-P. Wigneron, J.-M. Martinuzzi, J. Font, and M. Berger (2001), Soil moisture retrieval from space: The soil moisture and ocean salinity (SMOS) mission, *IEEE Trans. Geosci. Remote Sens.*, *39*, 1729–1735, doi:10.1109/36.942551.

Kool, J. B., and J. C. Parker (1988), Analysis of the inverse problem for transient unsaturated flow, *Water Resour. Res.*, *24*, 817–830, doi:10.1029/WR024i006p00817.

Kool, J. B., J. C. Parker, and M. T. Van Genuchten (1987), Parameter estimation for unsaturated flow and transport models: A review, *J. Hydrol.*, *91, 255–293, doi:10.1016/0022-1694 (87)90207-1.*

Krishnakumar, K. (1989), Microgenetic algorithms for stationary and nonstationary function optimization, *SPIE Intell. Control Adaptive Syst.*, *1196*, 289–296.

Leij, F. J., W. J. Alves, M. T. Van Genuchten, and J. R. Williams (1999), The UNSODA unsaturated soil hydraulic database, in *Characterization and Measurement of the Hydraulic Properties of Unsaturated Porous Media*, edited by M. T. Van Genuchten et al., pp. 1269–1281, Univ. of Calif., Riverside.

Mattikalli, N. M., E. T. Engman, T. J. Jackson, and L. R. Ahuja (1998), Microwave remote sensing of temporal variations of brightness temperature and near surface soil water content during a watershed-scale experiment, and its application to the estimation of soil physical properties, *Water Resour. Res.*, *34*, 2289–2299, doi:10.1029/98WR00553.

Michalewicz, Z. (1996), *Genetic Algorithms + Data Structures = Evolution Programs*, 3rd ed., Springer, New York.

Mohanty, B. P., and T. H. Skaggs (2001), Spatio-temporal evolution and time-stable characteristics of soil moisture within remote sensing footprints with varying soil, slope, and vegetation, *Adv. Water Resour.*, *24*, 1051–1067, doi:10.1016/S0309-1708(01)00034-3.

Mohanty, B. P., and J. Zhu (2007), Effective averaging schemes for hydraulic parameters in horizontally and vertically heterogeneous soils, *J. Hydrometeorol.*, *8*(4), 715–729, doi:10.1175/JHM606.1.

Mohanty, B. P., D. A. Miller, and M. T. Van Genuchten (2002), Soil property database: Southern Great Palins 1997 Hydrology Experiment, *Water Resour. Res.*, *38*(5), 1047, doi:10.1029/2000WR000076.

Mualem, Y. (1976), A new model for predicting the hydraulic conductivity of unsaturated porous media, *Water Resour. Res.*, *12*, 513–522, doi:10.1029/WR012i003p00513.

Njoku, E. G., T. J. Jackson, V. Lakshmi, T. K. Chan, and S. V. Nghiem (2003), Soil moisture retrieval from AMSR-E, *IEEE Trans. Geosci. Remote Sens.*, *41*, 215–229, doi:10.1109/TGRS.2002.808243.

Oliveira, R., and D. P. Loucks (1997), Operating rules for multireservoir systems, *Water Resour. Res.*, *33*, 839–852, doi:10.1029/96WR03745.

Ritzel, B., J. W. Eheart, and S. Ranjithan (1994), Using genetic algorithms to solve a multiobjective groundwater pollution containment problem, *Water Resour. Res.*, *30*, 1589–1603, doi:10.1029/93WR03511.

Romano, N., and A. Santini (1999), Determining soil hydraulic functions from evaporation experiments by a parameter estimation approach: Experimental verifications and numerical studies, *Water Resour. Res.*, *35*, 3343–3359, doi:10.1029/1999WR900155.

Russo, D., E. Bresler, U. Shani, and J. C. Parker (1991), Analyses of infiltration events in relation to determining soil hydraulic properties by inverse problem methodology, *Water Resour. Res.*, *27*, 1361–1373.

Sarwar, A., W. G. M. Bastiaanssen, M. T. Boers, and J. C. Van Dam (2000), Evaluating drainage design parameters for the fourth drainage project, Pakistan by using SWAP model: I. Calibration, *Irrig. Drain. Syst.*, *14*, 257–280, doi:10.1023/A:1006468905194.

Savic, D. and S.-T. Khu (2005), Evolutionary computing in hydrological sciences, in *Encyclopedia of Hydrological Sciences*, edited by M. G. Anderson, chap. 22, pp. 1–22, John Wiley, Hoboken, N.J.

Schaap, M. G., and F. J. Leij (2000), Improved prediction of unsaturated hydraulic conductivity with the Mualem-van Genuchten model, *Soil Sci. Soc. Am. J.*, *64*, 843–851.

Seibert, J. (2000), Multi-criteria calibration of a conceptual runoff model using a genetic algorithm, *Hydrol. Earth Syst. Sci.*, *4*, 215–224.

Šimůnek, J., O. Wendroth, and M. T. Van Genuchten (1998), Parameter estimation analysis of the evaporation method for determining soil hydraulic properties, *Soil Sci. Soc. Am. J.*, *62*, 894–905.

Singh, R., J. G. Kroes, J. C. Van Dam, and R. A. Feddes (2006a), Distributed ecohydrological modelling to evaluate the performance of irrigation system in Sirsa district, India: Current water management and its productivity, *I., J. Hydrol.*, *329*, 692–713, doi:10.1016/j.jhydrol.2006.03.037.

Singh, R., R. K. Jhorar, J. C. Van Dam, and R. A. Feddes (2006b), Distributed ecohydrological modelling to evaluate irrigation system performance in Sirsa district, India: II. Impact of viable water management scenarios, *J. Hydrol.*, *329*, 714–723, doi:10.1016/j.jhydrol.2006.03.016.

Van Dam, J. C. (2000), Field-scale water flow and solute transport: SWAP model concepts, parameter estimation and case studies, Ph.D. thesis, Wageningen Univ., Wageningen, Netherlands.

Van Dam, J. C., J. N. M. Stricker, and P. Droogers (1992), Inverse method for determining soil hydraulic functions from one-step outflow experiments, *Soil Sci. Soc. Am. J.*, *56*, 1042–1050.

Van Dam, J. C., J. N. M. Stricker, and P. Droogers (1994), Inverse method for determining soil hydraulic functions from multi-step outflow experiments, *Soil Sci. Soc. Am. J.*, *58*, 647–652.

Van Dam, J. C., J. Huygen, J. G. Wesseling, R. A. Feddes, P. Kabat, P. E. V. Van Waslum, P. Groenendjik, and C. A. Van Diepen (1997), Theory of SWAP version 2.0: Simulation of water flow and plant growth in the soil-water-atmosphere-plant environment, *Tech. Doc. 45*, Wageningen Agric. Univ. and DLO Winand Staring Cent., Wageningen, Netherlands.

Van Genuchten, M. T. (1980), A closed-form equation for predicting the hydraulic conductivity of unsaturated soils, *Soil Sci. Soc. Am. J.*, *44*, 892–898.

Vrugt, J. A., J. W. Hopmans, and J. Šimůnek (2001), Calibration of a two-dimensional root water uptake model, *Soil Sci. Soc. Am. J.*, *65*, 1027–1037.

Vrugt, J. A., C. G. H. Diks, H. V. Gupta, W. Bouten, and J. M. Verstraten (2005), Improved treatment of uncertainty in hydrologic modeling: Combining the strengths of global optimization and data assimilation, *Water Resour. Res.*, *41*, W01017, doi:10.1029/2004WR003059.

Walker, J. P., and P. R. Houser (2004), Requirements of a global near-surface soil moisture satellite mission: Accuracy, repeat time, and spatial resolution, *Adv. Water Resour.*, *27*, 785–801, doi:10.1016/j.advwatres.2004.05.006.

Walker, J. P., G. R. Willgoose, and J. T. Kalma (2001), One-dimensional soil moisture profile retrieval by assimilation of near-surface observations: A comparison of retrieval methods, *Adv. Water Resour.*, *24*, 631–650, doi:10.1016/S0309-1708(00)00043-9.

Wang, Q. J. (1991), The genetic algorithm and its application to calibrating conceptual rainfall-runoff models, *Water Resour. Res.*, *27*, 2467–2471, doi:10.1029/91WR01305.

Wardlaw, R., and M. Sharif (1999), Evaluation of genetic algorithms for optimal reservoir system operation, *J. Water Resour. Plann. Manage.*, *125*, 25–33, doi:10.1061/(ASCE)0733-9496(1999)125:1(25).

Wesseling, J. G. and J. G. Kroes (1998), A global sensitivity analysis of the model SWAP, *Rep. 160*, DLO Winand Staring Cent., Wageningen, Netherlands.

Wu, J., C. Zheng, C. Chein, and L. Zheng (2006), A comparative study of Monte Carlo simple genetic algorithm and noisy genetic algorithm for cost-effective sampling network design under uncertainty, *Adv. Water Resour.*, *29*, 899–911.

Xevi, E., J. Gilley, and J. Feyen (1996), Comparative study of two crop yield simulation models, *Agric. Water Manage.*, *30*, 155–173, doi:10.1016/0378-3774(95)01218-4.

Yang, K., T. Koike, B. Ye, and L. Bastidas (2005), Inverse analysis of the role of soil vertical heterogeneity in controlling surface soil state and energy partition, *J. Geophys. Res.*, *110*, D08101, doi:10.1029/2004JD005500.

Zhu, J., and B. P. Mohanty (2003), Effective hydraulic parameters for steady state vertical flow in heterogeneous soils, *Water Resour. Res.*, *39*(8), 1227, doi:10.1029/2002WR001831.

A. V. M. Ines, International Research Institute for Climate and Society, The Earth Institute at Columbia University, 61 Route 9W, Palisades, NY 10964, USA.

B. P. Mohanty, Department of Biological and Agricultural Engineering, Texas A&M University, 2117 TAMU, 201 Scoates Hall, College Station, TX 77843, USA. (bmohanty@tamu.edu)